UC Davis

UC Davis Previously Published Works

Title

A complex of Wnt/planar cell polarity signaling components Vangl1 and Fzd7 drives glioblastoma multiforme malignant properties

Permalink

https://escholarship.org/uc/item/5tp481f0

Authors

Dreyer, Courtney A

VanderVorst, Kacey

Natwick, Dean

et al.

Publication Date

2023-07-01

DOI

10.1016/j.canlet.2023.216280

Peer reviewed

A complex of Wnt/planar cell polarity signaling components Vangl1 and Fzd7 drives glioblastoma multiforme malignant properties

Courtney A. Dreyer[1], **Kacey VanderVorst**[1], **Dean Natwick**[2], **George Bell**[2], **Prachi Sood**[1], **Maria Hernandez**[1], **James M. Angelastro**[3], **Sean R. Collins**[2], **Kermit L. Carraway III**[1,*]

[1]Department of Biochemistry and Molecular Medicine and University of California Davis Comprehensive Cancer Center, University of California Davis School of Medicine, Sacramento, CA, USA

[2]Department of Microbiology and Molecular Genetics, University of California Davis, Davis, CA, USA

[3]Department of Molecular Biosciences, University of California Davis School of Veterinary Medicine, Davis, CA, USA

Abstract

Targeting common oncogenic drivers of glioblastoma multiforme (GBM) in patients has remained largely ineffective, raising the possibility that alternative pathways may contribute to tumor aggressiveness. Here we demonstrate that Vangl1 and Fzd7, components of the non-canonical Wnt planar cell polarity (Wnt/PCP) signaling pathway, promote GBM malignancy by driving cellular proliferation, migration, and invasiveness, and engage Rho GTPases to promote cytoskeletal rearrangements and actin dynamics in migrating GBM cells. Mechanistically, we uncover the existence of a novel Vangl1/Fzd7 complex at the leading edge of migrating GBM cells and propose that this complex is critical for the recruitment of downstream effectors to promote tumor progression. Moreover, we observe that depletion of *FZD7* results in a striking suppression of tumor growth and latency and extends overall survival in an intracranial mouse xenograft model. Our observations support a novel mechanism by which Wnt/PCP components Vangl1 and Fzd7 form a complex at the leading edge of migratory GBM cells to engage downstream effectors that promote actin cytoskeletal rearrangements dynamics. Our findings suggest that interference with Wnt/PCP pathway function may offer a novel therapeutic strategy for patients diagnosed with GBM.

*****Corresponding author:** Dr. Kermit L. Carraway III; Department of Biochemistry and Molecular Medicine and University of California Davis Comprehensive Cancer Center, University of California Davis School of Medicine, Sacramento, CA, 95817, USA; Tel: (916) 734-3114; klcarraway@ucdavis.edu.

Keywords

glioblastoma; noncanonical Wnt signaling; planar cell polarity; motility; proliferation

1. Introduction

Glioblastoma multiforme (GBM) is the most common and malignant form of brain cancer and is associated with high morbidity and mortality. Despite recent advances in the detection and treatment of these tumors the 5-year survival rate remains below 5%[1], substantially lower than most other solid tumor types. Currently, the standard therapeutic approach for patients diagnosed with GBM is multifaceted, employing surgical resection to remove the bulk of the tumor, followed by radiation and chemotherapy with temozolomide to eliminate residual cells[2]. Because GBM tumors are highly proliferative and infiltrative[3] tumor recurrence generally occurs in close proximity to the primary tumor site, and is often driven by subpopulations of residual cells that have disseminated into the surrounding brain tissue and evaded therapeutic intervention[4].

Common oncogenic drivers in GBM tumors, including epidermal growth factor receptor (EGFR) mutation and amplification, platelet-derived growth factor receptor (PDGFR) activation, and phosphatase and tensin homolog (PTEN) inactivation, contribute to GBM progression through downstream induction of phosphatidylinositol 3-kinase (PI3K)/Akt signaling, driving cellular proliferation and invasiveness[5-7]. However, therapeutic agents targeting these pathways have exhibited poor clinical efficacy[8-10], likely due to the highly heterogeneous nature of these tumors and their resistance to targeting of the presumed oncogene. Additional evidence suggests that activation of alternative molecular drivers may play a major role in the aggressive properties of GBM tumors.

Wnt/PCP is a branch of noncanonical Wnt signaling that is critical for normal development where it plays essential roles in mediating cell adhesion, tissue polarity, and migration, and requires the core components Vangl, Frizzled (Fzd), Prickle (Pk), and Dishevelled (Dvl)[11,12]. While Wnt/PCP has shared components with both canonical and other noncanonical Wnt signaling pathways, the presence and involvement of the transmembrane scaffold Vangl distinguishes Wnt/PCP signaling from other Wnt pathways and is essential for proper pathway function[13-15]. Activation of Wnt/PCP signaling occurs upon binding of a non-canonical Wnt ligand, such as Wnt5a, to a Fzd receptor at the plasma membrane. This results in the recruitment of Dvl and its subsequent phosphorylation, allowing Dvl to engage downstream effectors including Rho GTPases and c-Jun N Terminal Kinase (JNK) to drive cytoskeletal rearrangements and actin dynamics[14].

Given that developmental pathways are often hijacked and reactivated by tumors to drive malignancy, it comes as no surprise that core Wnt/PCP components are dysregulated in several cancer types and contribute to tumor progression[13-16]. Of note, we previously reported that transcript levels of Wnt/PCP components *VANGL1, FZD7,* and *WNT5A* are all upregulated in GBM tumors relative to normal tissue regardless of tumor subtype, and their high expression levels correlate with poorer patient outcome[17]. Further, we identified a mechanism by which the E3 ubiquitin ligase Nrdp1 negatively regulates Wnt/PCP signaling

in GBM cells. Nrdp1 interaction with Vangl1 and Vangl2 impairs Dvl localization to the cell membrane through K63-linked polyubiquitination, preventing the propagation of downstream signaling[17]. However, the direct involvement of the core Wnt/PCP components and their contribution to GBM cellular invasiveness and hyper-proliferation has not yet been extensively studied in GBM.

Here we report a mechanism by which Wnt/PCP signaling mediates the aggressive properties of GBM tumors. We demonstrate that Wnt/PCP components Vangl1 and Fzd7 localize to and complex at the leading edge of motile GBM cells to promote cell proliferation, motility, and invasiveness by engaging downstream Rho GTPases to mediate cytoskeletal rearrangements and actin dynamics. Further, we show that Fzd7 is critical to GBM tumor growth and aggressiveness *in vivo.* Our results identify a novel mechanism by which an understudied developmental pathway contributes to the aggressive properties of GBM tumors and reveal novel opportunities for successful therapeutic intervention for patients diagnosed with GBM.

2. Materials and Methods

2.1 Cell Culture and Reagents

U251 and LN229 cells were a kind gift from Dr. Paul Knoepfler. The patient-derived xenograft (PDX) line, GBM12, was obtained from Mayo Clinic, and HEK293T cells were purchased from American Type Cell Collection (ATCC). Cell lines were authenticated by short-tandem repeat profiling (Genetics Core Facility at University of Arizona) and tested for mycoplasma contamination by RT-PCR[18,19], prior to, and at the conclusion of use in the outlined studies. Cell lines were cultured in Dulbecco's Modified Eagle Medium (DMEM) with L-Glutamine (Gibco) supplemented with 10% fetal bovine serum (Genesee) and 1% penicillin-streptomycin (Genesee) and were maintained at 37°C in 10% CO_2 as recommended. Antibodies used are as follows: anti-NCAM1, anti-phospho-β-catenin (Ser33/37/Thr41), β-catenin, anti-HA-Tag, and anti-Flag (Cell Signaling), anti-Vangl1 (R&D Systems), anti-Fzd7 and anti-Dvl2 (Abcam), anti-Flag and anti-Actin (Sigma), anti-phospho-Vangl2 (Thr78, Ser79, Ser82) (ThermoFisher), anti-Vangl2 (Proteintech), anti-Phalloidin647, 4′,6-diamidino-2-phenylindole (DAPI), and Alexa-Fluor 488-conjugated goat anti-mouse, Alexa-Fluor 488-conjugated goat anti-rabbit, and Alexa-Fluor 546-conjugated goat anti-rabbit secondary antibodies (Invitrogen), horseradish peroxidase-conjugated goat anti-mouse and anti-rabbit secondary antibodies (Bio-Rad). Protein G Plus/Protein A Agarose Suspension was purchased from Millipore/Sigma. A/C Heterodimerizer was purchased from Takara.

2.2 Generation of stable knockdown and overexpression cell lines

Stable cell lines were generated by lentiviral transduction. *VANGL1*-targeted shRNA constructs employed are as follows: shVangl1-1 (Clone ID: TRCN0000062089), shVangl1-2 (Clone ID: TRCN0000062090), and shVangl1-3 (Clone ID: TRCN0000062092) (Dharmacon). *FZD7*-targeted shRNA constructs employed are as follows: shFzd7-1 (Clone ID: TRCN0000008344), and shFzd7-2 (Clone ID: TRCN0000008345) (Dharmacon). pLKO.1 scramble shRNA (a gift from David Sabatini, Addgene plasmid #1864; http://

n2t.net/addgene:1864; RRID:Addgene_1864)[20] was employed as the shControl vector. Stable overexpression lines were created using a LifeAct-GFP plasmid that was a gift from Mary Beckerle (Addgene plasmid #187686; http://n2t.net/addgene:187686; RRID:Addgene_187686)[21], a luciferase-EGFP plasmid that was a gift from Fernando Fierro (Addgene plasmid #89608; http://n2t.net/addgene:89608; RRID:Addgene_89608)[22], or an mCherry plasmid that was a gift from Pantelis Tsoulfas (Addgene plasmid #36084; http://n2t.net/addgene:36084; RRID:Addgene_36084). VSVG-pseudotyped virus was generated in HEK293T cells by transfecting with the psPax2 packaging vector. Cells were transduced with 10μg/mL polybrene (Millipore) and were drug-selected with 1μg/mL puromycin (Sigma), 4μg/mL blasticidin (Sigma), or 200μg/mL hygromycin B (ThermoFisher), or sorted by EGFP with a BD "inFlux" 18-color cell sorter (Becton Dicksinson).

2.3 Proliferation and motility assays

To measure cell proliferation, cells were seeded and fixed at 0, 24, 48, and 72 hours of proliferation, stained with DAPI, and then imaged and counted. The number of cells counted at each time point was normalized to 0 hour to generate growth curves over time. For scratch migration assays, confluent monolayers of cells were scratched with a sterile pipette tip and imaged at 0- and 12-hours post-scratch. ImageJ (NIH) was used to measure the difference in scratch area over 12 hours. For Boyden chamber assays, cells were seeded into an 8μm pore polycarbonate membrane (Corning) in DMEM supplemented with 0.01% fetal bovine serum and allowed to migrate for 18 hours towards the lower chamber containing DMEM supplemented with 10% fetal bovine serum. Cells migrated through the membrane were stained with Diff-Quick staining solution (Dade Behring), imaged, and counted. Results were normalized to proliferation rates and respective controls for all experiments. All imaging was done using an Olympus IX81 inverted microscope with CellSens Entry software.

2.4 qRT-PCR

Total RNA was isolated using a PureLink RNA MiniKit (Ambion) and DNaseI treated (Sigma) according to the manufacturer's protocols. Complementary DNA was generated using the High-Capacity complementary DNA reverse transcription kit (Applied Biosystems). Quantitative real-time PCR was performed using SsoAdvanced Universal Probes Supermix (Bio-Rad) and gene-specific TaqMan primer/probes sets (ThermoFisher) in a Bio-Rad iCycler CFX-96 real-time PCR machine. Transcript levels for *hVANGL1* (Hs01572998_m1), *hVANGL2* (Hs00393412_m1), *hWNT5A* (Hs00998537_m1), *hPK1* (Hs01055551_m1), *hNRDP1/RNF41* (Hs00195064_m1), and *hFZD7* (Hs00275833_s1) were analyzed using Bio-Rad CFX Manager software and normalized to human glyceraldehyde-3-phosphate dehydrogenase (*hGAPDH,* Hs02786624_g1) for each sample.

2.5 Ex vivo organotypic brain slice assays and in vitro 3D collagen I invasion assays

All animal studies were conducted according to approved protocols by the IACUC of the University of California, Davis, USA. To assess cell invasion e*x vivo,* organotypic brain slices assays were conducted as described[23]. Briefly, 8- to 12-week-old FVB mice were euthanized, the brain was immediately dissected out, and 1mm coronal slices were made using a mouse brain slicer (Braintree Scientific, Inc.) under sterile conditions.

Brain slices were cultured in transwells with 0.4μm polycarbonate membranes in a plate containing culture medium consisting of 50% Minimum Essential Medium (MEM)(Gibco), 25% Hank's Balance Salt Buffer (HBSS)(Gibco), 25% Horse Serum (Invitrogen), 1% penicillin-streptomycin (Genesee), 1% MEM Nonessential Amino Acids (NEAA) (Gibco), and 50μg/mL Gentamicin (Genesee). GBM spheroids expressing mCherry were generated by seeding into ultra-low attachment plates (Corning) and cultured in Neurobasal media (Gibco) supplemented with 1X B27 (Invitrogen), 20μg/mL epidermal growth factor (EGF) (ThermoFisher), 20μg/mL fibroblast growth factor (FGF)(Corning), 50mg/mL heparin (Sigma), 200nM L-glutamine (Sigma), and 1% penicillin-streptomycin (Genesee). Spheres were collected and manually implanted into mouse brain slices using a 10μL pipette under a microscope. Three days post-implantation, brain slices were fixed in 4% paraformaldehyde overnight, and the tissue was cleared using the SeeDB protocol[24]. For *in vitro* sphere invasion assays in collagen I, GBM spheroids were generated and twenty-four hours later, collected and embedded into rat-tail collagen I (ThermoFisher) as previously described[25]. Spheroids in collagen I were fixed after 24 hours in 4% paraformaldehyde. Brain slices and spheres in collagen were imaged using a Zeiss LSM 800 AxioObserver confocal microscope and quantified using Zen Blue v3.3 software. Infiltrated cells were visualized as spikes exiting from the bulk of the spheroid. Approximate sphere volumes were determined using the equation $V=(W^2xL)/2$, and distance invaded was determined by measuring the length from the sphere perimeter to the center of mass of the cell. The average number of cells invaded was normalized to approximate sphere volume to consider slight differences in spheroid sizes across groups. Results were normalized to their respective controls across independent experiments.

2.6 Immunofluorescence staining and LifeAct-GFP Imaging

Cells seeded onto coverslips, spheroids, or spheroids embedded in collagen I were fixed with 4% paraformaldehyde, stained with the antibodies indicated, and imaged using a Zeiss LSM 800 AxioObserver confocal microscope or a Keyence BZ-X810 microscope. A secondary antibody only control was included for each experiment. Spheroids stained for NCAM1 were analyzed using ImageJ to quantify the mean intensity of NCAM1 signal. Colocalization analysis of immunofluorescence staining was carried out using the Coloc2 plugin in Fiji to calculate Pearson's correlation coefficient (r). Regions of interest (ROIs) were drawn around the protrusive front of the cell and further divided into smaller ROIs within the cellular protrusion around areas of enriched F-actin, to specifically assess colocalization of proteins within these structures. For LifeAct-GFP imaging and analysis, cells were seeded onto coverslips, and when confluent were scratched with a sterile pipette tip and allowed to migrate for 12 hours, followed by fixation in 4% paraformaldehyde. Fixed cells were stained with DAPI and imaged using a Zeiss LSM 800 AxioObserver confocal microscope. The percentage of cells with F-actin-enriched protrusions was quantified by counting the number of cells with and without F-actin-enriched cell fronts along the edge of the scratch by assessing differences in signal intensity from 5 independent experiments.

2.7 FRET biosensor low confluency migration assay and high-magnification spatial imaging and analysis

U251 cells stably knocked down for Vangl1 or Fzd7 were subsequently stably transfected with Rac1 or RhoA intramolecular FRET biosensors, which have been previously described[26,27]. Cells containing Rac1 or RhoA biosensors were sorted with a BD "inFlux" 18-color cell sorter (Becton Dickinson). Cells were plated in glass bottom 96-well plates (Cellvis), and once adhered the media was changed to Liebovitz-15 (L-15) media with no riboflavin, folic acid, or dyes (UC Davis Biological Media Services), and supplemented with 2% fetal bovine serum for imaging. All imaging experiments were performed using a Nikon Eclipse TI microscope equipped with an OKO Labs incubator at 37 C, a 20x Nikon Apochromat 0.75 NA objective or 60x 1.49 NA Nikon Apochromat objective, an X-Cite XLED1 illumination module, dual Andor Zyla 4.2 sCMOS cameras, and a Cairn TwinCam LS image splitter with a Chroma Technologies dichroic mirror (ZT481 rdc) for simultaneous acquisition of FRET images. The microscope was controlled via custom software using MATLAB through Micro-Manager (v 1.4). For low confluency FRET imaging and analysis, the XY positions for each well were set manually and stored in MATLAB for timelapse imaging of the same field of view. Epifluorescent CFP and YFP images were collected every 15 minutes for 10 hours using a 20x Nikon Apochromat 0.75 NA objective, with ~450nm excitation illumination provided by the X-Cite XLED1 BLX module. Camera and illumination corrections, imagine alignment, background subtraction, and segmentation were carried out using previously described methods[16]. The average FRET ratio in each field of view was calculated, and the compiled measurements were normalized according to the measurement at the initial time point and plotted as the average FRET ratio over time. For high magnification spatial Rac1 FRET imaging experiments, each well was organized into an x-y grid of predefined locations, and a single cell was manually chosen for imaging at each location. Automated epifluorescent CFP and YFP images were collected every 10 seconds for 10 minutes using a 60x objective with 445nm excitation illumination provided by the X-Cite XLED1 BLX module.

2.8 Camera corrections, image alignment, background subtraction, and cell segmentation for high-magnification spatial imaging

Image processing steps were performed using MATLAB. First, the dark-state noise for each camera was empirically measured as described by Bell et al.[28]. Briefly, several images were captured without illumination and the microscope light path set to the oculars. The dark-state correction image was generated by taking the median over the stack of dark images. The appropriate correction for each camera was subtracted from all raw CFP and YFP images. Next, CFP and YFP images were aligned using a custom alignment algorithm described by Bell et al.[28], then cropped to a standard size. After alignment, CFP and YFP images were summed to increase the signal-to-noise ratio for segmentation. Local background subtraction was performed on summed images by isolating non-cell pixels using an initial conservative cell segmentation to remove high intensity pixels, then calculating the median intensity of pixels within 300 x 300 pixel blocks. Smoothing was applied to remove hard edges and generate smooth background images that were subtracted from the summed images. Next, pixels above an empirically determined upper threshold were reduced to flatten images for segmentation purposes. Importantly, this step was not performed on

images used for FRET ratio calculations. Images were then smoothed using a Gaussian filter of width 5 pixels and sigma 2 pixels and cell edges were enhanced using unsharp masking with a broad Gaussian filter of width 10 pixels and sigma 75 pixels. Cell segmentation was performed using automated pixel thresholding, removal of small debris (<25 pixels) using MATLAB's "bwareaopen" function, morphological closing using MATLAB's "imdilate" and "imerode" functions, filling holes in cell masks using MATLAB's "imfill" function, removal of non-cell objects (<5000 pixels), and removal of cell masks touching the image border using MATLAB's "imclearborder" function. To create FRET ratio images, after application of camera corrections and image alignment, background subtraction was performed on individual CFP and YFP images using the methodology described above. Finally, for both CFP and YFP images, cell masks were applied by setting background pixels to NaN, images were smoothed using a Gaussian filter of width 7 pixels and sigma 2 pixels, cell masks were reapplied post-smoothing, then FRET ratio images were generated by performing pixel-by-pixel division of the YFP image by the CFP image.

2.9 Determination of data points for quantification for high-magnification spatial imaging

Image analysis and quantification steps were performed using MATLAB. Cells displayed a range of morphologies and migratory phenotypes on our high magnification imaging experiments. For quantification of spatial FRET activity, we focused our analysis on cells and timepoints in which cells migrated with a primary protrusion and retraction located opposite each other along the cell's polarity axis. To isolate these data points, we calculated each cell's centroid speed and x and y displacements over the entire time course and plotted these data alongside images of each cell's mask perimeter, largest protrusion, and largest retraction overlayed over the entire time course. To locate the largest protrusion and retraction for each cell, we subtracted each mask from the mask 30 seconds prior, associated protrusions with pixels of value 1 and retractions with pixels of value −1, then identified the largest connected pixel regions of each value. Based on the visual representations described above, the appropriate frames were manually selected for each cell.

2.10 Quantification of front-back FRET ratio gradients for high-magnification spatial imaging

The Rac1 spatial activity gradient was calculated from FRET images corresponding to the chosen data points as previously described[29]. Briefly, for each frame, the central edge pixel within the cell protrusion was located by identifying the edge pixels within the largest protrusion then calculating the median pixel within this group. All pixels in the cell mask were then binned according to their geodesic distance from the central edge pixel using MATLAB's "bwdistgeodesic" function with a bin width of 3.75 pixels. The mean FRET value of each bin was calculated to determine the Rac1 activity gradient of each cell on a frame-by-frame basis. A final Rac1 activity gradient was calculated for each cell by taking the mean activity gradient across all time points.

2.11 Quantification of cell-wide, protrusion, and retraction FRET ratios for high-magnification spatial imaging

The cell-wide Rac1 FRET ratio of each cell was determined by calculating the mean FRET ratio within the cell mask for each timepoint, then calculating the mean value across all

timepoints. For protrusion and retraction FRET calculations, we identified the edge pixels within the largest protrusion and retraction of the cell at each timepoint, and protrusion and retraction pixels were defined as the 10% of pixels nearest to the protrusion and retraction edge pixels, respectively. The protrusion and retraction FRET ratio of each cell was determined by calculating the mean FRET ratio within the protrusion and retraction pixels, respectively, for each timepoint, then calculating the mean value across all timepoints.

2.12 Co-immunoprecipitation and immunoblotting

Cells were lysed in 2x Laemmli buffer or in co-immunoprecipitation buffer with phosphatase and protease inhibitors. Co-immunoprecipitations and immunoblotting were performed as previously described[30,31]. Pierce Supersignal West Femto Maximum Sensitivity Substrate or Pierce ECL Western Blotting Substrate (ThermoFisher) were used to develop immunoblots on a myECL Imager (ThermoFisher). Band density was quantified using ImageJ and normalized to actin as a loading control.

2.13 Proximity Ligation Assay

Cells seeded onto coverslips were fixed in 4% paraformaldehyde and the Duolink Proximity ligation assay (Duolink *In Situ* Red Starter Kit Mouse/Rabbit - Sigma) was used to assess protein-protein interactions. The assay was performed according to manufacturer's specifications. Briefly, coverslips were blocked, primary antibodies raised in different species were applied, followed by incubation with PLA probes detecting mouse and rabbit. Probes were then ligated, and the closed circular DNA template was amplified with a DNA polymerase resulting in discrete fluorescent puncta that could be visualized under the microscope. Coverslips were mounted onto slides with *In Situ* Mounting Medium with DAPI (Sigma) and imaged on a Keyence BZ-X810 microscope. PLA images were quantified using ImageJ by calculating the area of PLA signal per field of view normalized to cell number, for each condition.

2.14 Generation of Vangl1 and Fzd7 iDimerize lines

The Lenti-X iDimerize Inducible Heterodimer system[32] (Takara) was employed to induce Vangl1-Fzd7 protein-protein interactions. Flag-Vangl1 and Fzd7-HA constructs described previously[17], were subcloned into pLVX-Het1-DmrC or pLVX-Het2-DmrA, respectively, using In-Fusion Snap Assembly (Takara) to produce pLVX-Het1-DmrC-Flag-Vangl1 and Het2-Fzd7-HA-DmrA constructs. Lentiviral particles were produced as described above and used to transduce U251 or LN229 cells, followed by selection with antibiotics. Cells were treated with A/C Heterodimerizer (A/C) (Takara) at 50nM for functional assays.

2.15 Generation of intracranial xenografts in mice

Animal studies were conducted according to protocols approved by the IACUC of the University of California, Davis, USA. Male and female NOD.Cg-*Prkdc*^*scid*^/J (NOD SCID) mice, aged 8 to 12 weeks (The Jackson Laboratory) were anesthetized and placed into a Kopf stereotaxic apparatus. A sagittal incision was made in the scalp to expose the skull, and access to the brain was achieved by drilling a hole 1mm in diameter located 1mm anterior, 1mm lateral, and 2mm deep relative to the bregma where 1×10^4 cells were stereotactically

injected in 1μL of volume using a 5μL Hamilton syringe. Tumor growth was monitored via bioluminescence imaging. Mice were sacrificed when moribund behavior was observed, or at a maximum of 120 days from the first observation of tumor by bioluminescence imaging. At endpoint, mice were anesthetized and transcardially perfused with fixative, and the brains were removed and fixed overnight at 4°C. Brains were either paraffin embedded and sectioned, or cryoprotected in 30% sucrose, snap frozen in OCT compound, and cryosectioned. Sections were processed for histological analysis.

2.16 In vivo bioluminescence monitoring of tumor growth and analysis

Mice bearing intracranial xenograft tumors were imaged weekly following completion of post-operation monitoring. Mice were anesthetized, given an intraperitoneal injection with 30mg/mL RediJect D-luciferin (Perkin-Elmer), placed in the IVIS Spectrum (Perkin-Elmer), and imaged 5 minutes post-injection to obtain an intensity map representing the approximate tumor size. Quantification of the bioluminescence signal was performed using Aura software (Spectral Instruments Imaging) and expressed as total flux (photons per second).

2.17 MR Imaging of tumor growth

MRI scans of mice bearing intracranial tumors was performed at 60 days post-tumor cell engraftment. Imaging was performed at the Center for Molecular and Genomic Imaging with a Bruker Biospec 70/30 (7T) preclinical MR scanner (Bruker BioSpin MRI, Ettlingen Germany) equipped with a 116 mm internal diameter B-GA12S gradient (450 mT/m, 4500 T/m/s), a 72 mm internal diameter (ID) linear transmit coil, and a 20 mm ID surface coil for signal reception. Paravision 6.0 (Bruker BioSpin, MRI) software was used for acquisition, reconstruction, and analysis. Immediately prior to imaging, animals were anesthetized with isoflurane/O_2 (Piramal Healthcare, Bethlehem PA) using 2.0% vol/vol to induce and 0.5%–1.5% vol/vol to maintain anesthesia. Once anesthetized, animals were stereotactically restrained, and imaged for ~30 minutes. Temperature and respiration rate were monitored using SAII (Small Animal Instruments, Inc, Stony Brook, New York) small-animal monitoring equipment, and maintained using warm air and adjustments to isoflurane dose. Multislice, T_2-weighted Rapid Acquisition with Repeated Echoes (RARE) trans-axial images with the following parameters: repetition time (TR) = 6000 ms; effective echo time (TE) = 54 ms; RARE factor = 8; averages = 8; in-plane data matrix of 160×160 with resolution of 0.125×0.125 mm^2; 35 slices with a 0.25 mm thickness.

2.18 Histology and immunohistochemistry

Mouse brains were processed for histologic analysis and sections were stained with hematoxylin and eosin (H&E), or subject to immunohistochemical (IHC) staining as described previously[33,34]. Secondary antibody only controls were included in each experiment. Images were captured with a Keyence BZ-X810 microscope and stitched together using BZ-X800 analyzer software. Ki67 staining was quantified by counting the number of Ki67^{+} cells in each field of view.

2.19 Statistical Analysis

All data was analyzed across at least three independent experiments. Statistical analysis was performed using GraphPad Prism software. Statistical significance was determined using unpaired two-tailed t-tests with Welch's correction, paired t-tests, ordinary one-way ANOVAs, or Mann-Whitney tests. Kaplan-Meier analysis was used to estimate survival and a Log-rank test was performed to determine differences in survival between groups. Details of statistical tests employed are stated in the figure legends and text. P-values <0.05 were determined to be statistically significant (ns=not significant, $*p < 0.05$; $**p < 0.01$; $***p < 0.001$; $****p < 0.0001$).

2.20 Data Availability

The data presented is included in the article and can also be made available upon request.

3.   Results

3.1   Wnt/PCP components Vangl1 and Fzd7 promote glioblastoma cell growth and migration

The highly infiltrative and proliferative nature[3] of GBM is most often attributed to growth factor/receptor tyrosine kinase (GF/RTK) pathways[35], but other mechanisms have not been excluded. We profiled the expression of Wnt/PCP components *VANGL1*, *FZD7*, and *WNT5A* and observed the presence of these transcripts across the conventional GBM cell lines: U251 and LN229, and in the patient-derived xenograft (PDX) line GBM12 (Supplementary Fig. 1). Further analysis revealed that other Wnt/PCP pathway members including *VANGL2, NRDP1, and PRICKLE1*, are also detectable (Supplementary Fig. 1). These GBM cell models were used in the present study because they retain many of the characteristics of human disease when orthotopically xenografted into mice[35-38], and can be manipulated in culture to study biological effects due to perturbation of Wnt/PCP components.

To assess the role of Wnt/PCP signaling in promoting GBM malignancy, we first investigated the contribution of dysregulated Wnt/PCP components Vangl1 and Fzd7 to GBM cell proliferation *in vitro*. Suppression of *VANGL1* or *FZD7* exhibits a significant decrease in cellular proliferation over 48-72 hours, an effect that was consistent across both GBM cell lines stably expressing multiple short hairpin RNAs (shRNAs) sequences (Fig. 1A-B, Supplementary Fig. S2A-B). Suppression of *VANGL1* or *FZD7* expression was confirmed by RT-*q*PCR (Supplementary Fig. 3A-B).

Wnt/PCP has been reported to mediate cellular motility in various tumor types[39-41], leading us to next interrogate the role of Wnt/PCP components Vangl1 and Fzd7 in promoting GBM cell migration. We found that loss of *VANGL1* or *FZD7* expression significantly impairs the ability of GBM cells to migrate in a scratch assay (Fig. 1C-F). GBM tumor cells can infiltrate out of the primary tumor as single cells[42] or semi-collectively, as multicellular streams, and invade along chemoattractant secreting white matter tracts[45]. Thus, we employed transwell Boyden assays as a complementary method to assess the role of Wnt/PCP components in GBM cell migration toward a growth factor gradient. We

observed that depletion of *VANGL1* or *FZD7* expression significantly suppresses GBM cell migration through the transwell filter (Fig. 1G-J). To exclude the possibility that differences observed in migration were due to cell proliferation we carried out proliferation assays on the same abbreviated timescales as the migration assays and observed no significant differences in proliferation between control and *VANGL1* or *FZD7* depleted cells over 12 hours (Supplementary Fig. 3C-D). Combined, these data reveal a role for Wnt/PCP components Vangl1 and Fzd7 in mediating key cellular behaviors that promote the aggressive properties of GBM tumors.

3.2 Wnt/PCP components Vangl1 and Fzd7 drive glioblastoma cell invasiveness

GBM tumor cells characteristically invade through the perivascular space and brain parenchyma, which requires GBM cells to invade through both extracellular matrix (ECM) and normal brain tissue. To investigate the role of Wnt/PCP components Vangl1 and Fzd7 in GBM invasion into a 3D ECM-like matrix, we first employed an *in vitro* Collagen I invasion assay. Here, U251-mCherry spheroids were embedded into a collagen I matrix and invasion was assessed after 72 hours. We observed that depletion of *VANGL1* or *FZD7* significantly reduces the number of cells invading out of the spheroid, as well as the relative distance that cells invade into the surrounding collagen I matrix (Supplementary Fig. S4A-F).

Because Wnt/PCP signaling has been previously reported to regulate cell-cell adhesions[46,47] we assessed expression of neural cell adhesion molecule 1 (NCAM1), a cell surface glycoprotein that mediates cell-cell and cell-ECM interactions in the brain[48], by immunofluorescence and observed no significant differences in expression between control and *VANGL1* or *FZD7* knockdown spheroids (Supplementary Fig. S5A-C). Further, spheroids were assessed for Vangl1 and Fzd7 expression, which are expressed throughout the bulk of the spheroids (Supplementary Fig. S5D-E). Of interest, staining of invaded spheroids in collagen I for Vangl1 and Fzd7 revealed that component expression is maintained in invading cells (Supplementary Fig. S6A-B), highlighting their potential importance in mediating GBM cell invasion.

To better recapitulate the environment in which GBM cells invade *in vivo*, we employed an *ex vivo* organotypic brain slice assay[23]. This model more closely mimics the 3D environment that GBM tumor cells encounter *in vivo* by providing distinct anatomical features of brain tissue and interactions with other cell types, both of which are challenging to replicate using other *in vitro* models and are critical factors that influence GBM cell invasiveness[45]. Here, U251-mCherry spheroids were implanted into mouse brain slices and allowed to invade for 72 hours (Fig. 2A). We observed that depletion of *VANGL1* or *FZD7* expression significantly reduces GBM invasion into mouse brain slices, reducing both the distance cells invade out of spheroids, as well as the number of cells that invade out of spheroids (Fig. 2B-G).

Collectively, this comprehensive dataset provides substantive evidence that Wnt/PCP components Vangl1 and Fzd7 promote GBM cell invasiveness.

3.3   Vangl1 and Fzd7 mediate downstream Rho GTPase activity in migrating glioblastoma cells

Cell migration is a tightly regulated and cyclic process whereby cells extend leading-edge protrusions, adhere to the ECM, and disassemble and detach the rear-end of the cell to drive forward movement[49]. The extension of cellular protrusions and establishment of cell polarity critical for cell migration are largely regulated by Rho family GTPases which are central mediators of cytoskeletal reorganization[50]. The Rho GTPases Rac1 and RhoA have been previously implicated as important downstream effectors of Wnt/PCP in cell migratory events in development[51,52], and in cancer[17,53,54]. Indeed, we previously established that overexpression of the E3 ubiquitin ligase Nrdp1, a negative regulator of Wnt/PCP signaling, significantly decreases the amounts of active RhoA in GBM cells using GST pull-down assays[17]. However, both the kinetics and subcellular localization of Rho GTPase activities downstream of Vangl1 and Fzd7 during GBM cell migration remain unclear.

To gain a deeper understanding of how Wnt/PCP components engage downstream Rho GTPase activity in real time, we employed Rac1 and RhoA FRET biosensors to assess temporal dynamics of GTPase activity upon perturbation of Vangl1 or Fzd7. Here, Rac1 or RhoA intramolecular biosensors were stably introduced into U251 cells depleted of *VANGL1* or *FZD7*, and their activities in migrating cells were monitored using live cell FRET imaging (Fig. 3A). In control cells, we observed an increase in Rac1 activity over ten hours of migration, whereas knockdown of *VANGL1* or *FZD7* exhibited both reduced basal Rac1 activity levels and diminished increase in Rac1 activity over time (Fig. 3B-E, Supplementary Fig. S7A-B). Importantly, we found that overall RhoA activity decreased over time in migrating control cells, consistent with previous reports[55]. However, in line with our findings with Rac1, RhoA activity was significantly lower for cells with knockdown of *VANGL1* or *FZD7* compared to control cells throughout the time course, including the basal activity levels (Supplementary Fig. S7C-F).

To further investigate the engagement of Rho GTPases during GBM cell migration, we employed high-magnification spatial analysis to assess the subcellular localization of Rac1 activity in migrating cells. We evaluated the spatial activity profile of Rac1 as a function of the distance from the leading edge in migratory GBM cells[29] and found that Rac1 activity is highest at the protrusive cell front and steadily decreases towards the rear of the cell (Fig. 3F-G, Supplementary Fig. 7G). Indeed, a comparison of Rac1 activity stratified by cell region indicates that active Rac1 is significantly enriched in cellular protrusions compared to the cell-wide average Rac1 activity, and it is significantly depleted in areas of cell retraction (Fig. 3H). Together, these observations indicate that Rac1 activity is enriched in cellular protrusions of migratory GBM cells, and that Wnt/PCP components Vangl1 and Fzd7 regulate Rac1 and RhoA activity to drive GBM cell motility.

3.4   Vangl1 and Fzd7 regulate actin cytoskeletal rearrangements critical to cell motility

Our observations that Wnt/PCP components Vangl1 and Fzd7 regulate downstream signaling through Rho GTPase activity led us to next examine their role in mediating cytoskeletal rearrangements and actin dynamics. Here, we employed the LifeAct-GFP system[56] to assess actin dynamics in real-time in migrating U251 and LN229 cells in a

scratch assay format. We observed that *VANGL1* or *FZD7* depletion reduces the percentage of cells at the edge of the scratch with F-actin-enriched cellular protrusions (Fig. 4A-D), an indication that cells depleted of *VANGL1* or *FZD7* are likely less motile[57]. These data suggest that Wnt/PCP components Vangl1 and Fzd7 are responsible for regulating cytoskeletal rearrangements and actin dynamics, which are critical drivers of cell motility in GBM cells.

3.5 Wnt/PCP components Vangl1 and Fzd7 interact to regulate downstream signaling and GBM cell motility

To begin to characterize the molecular underpinnings by which Wnt/PCP components Vangl1 and Fzd7 engage downstream effectors to regulate cytoskeletal rearrangements and actin dynamics critical to cell motility, we first aimed to assess the subcellular localization of Wnt/PCP components in migrating GBM cells. During development, PCP is required for the establishment and maintenance of planar polarity across epithelial tissues[11]. In this context it is well-established that PCP components localize asymmetrically, with Vangl/Pk complexes at the proximal side of the cell and Fzd/Dvl complexes at the distal side[58-61]. This asymmetry is in turn propagated to neighboring cells through protein-protein interactions to establish polarity across an epithelial sheet[62-65]. However, it remains unclear if the core component asymmetry required for tissue polarity is conserved in migrating cells. Most published reports on PCP subcellular localization are in breast cancer cells[39,40], where the subcellular localization of complexes remains disputed, and the question has not been addressed in GBM cells.

We assessed subcellular localization of endogenous Wnt/PCP components in migratory GBM cells by fluorescence microscopy. In migrating U251 cells, we observed that a fraction of both endogenous Vangl1 and Fzd7 localize sharply to F-actin-rich cellular protrusions (Fig. 5A). Moreover, we detected partial overlap in Vangl1 and Fzd7 staining, resulting in the formation of yellow puncta in merged images (white arrows), indicating that the two proteins are very closely associated with one another and may physically interact. U251 cells were also co-stained for Vangl1 and Dvl2 (Supplementary Fig. S8). While Dvl2 is predominantly localized in the cytosol, there is some enrichment of Dvl2 at the cell membrane co-localized with Vangl1, consistent with previous reports that Vangl is able to recruit Dvl to the cell membrane[59]. Further analysis revealed a positive correlation between both Vangl1 and Fzd7 (Supplementary Fig. 9A-C), and Vangl1 and Dvl2 (Supplementary Fig. 9D-F) at the leading edge of migratory GBM cells.

The observed co-localization of Vangl1 and Fzd7 in migratory GBM cells led us to speculate that Vangl1 and Fzd7 may form a complex at the leading edge of migrating cells to promote downstream signaling events that regulate actin-dynamics and cytoskeletal rearrangements. When co-transfected into HEK293T cells, we observed that Fzd7 co-immunoprecipitates with Vangl1 (Fig. 5B), suggesting that the two proteins are able to physically interact and consistent with other reports[66]. Next, to elucidate whether Vangl1 and Fzd7 can interact endogenously and intracellularly, we performed a proximity ligation assay (PLA) *in situ*. In U251-LifeAct-GFP cells, we were able to detect endogenous protein-protein interactions between Vangl1 and Fzd7 (Fig 5C). Notably, Vangl1-Fzd7 interactions were observed at

the leading edge of migratory cells, suggesting that this interaction may be important in recruiting and activating downstream effectors at sites of cellular protrusions to drive motility. U251-LifeAct-GFP cells stained only with Vangl1 or Fzd7 alone resulted in no detection of protein-protein interactions, similar to a secondary antibody only control (Supplementary Fig. S10A-B), demonstrating that Vang1 and Fzd7 interact endogenously in single migratory GBM cells.

To investigate the contribution of Vangl1 and Fzd7 to downstream outcomes, we first assessed their role in mediating pathway activation. Phosphorylation of Vangl has been well-established as being required for both proper localization of Vangl and pathway function[67-69]. Studies have shown that Wnt5a can induce Vangl phosphorylation to yield critical downstream outcomes during development[67,69,70], suggesting that phosphorylation of Vangl is indicative of pathway activation. We stably co-overexpressed Vector/Vector, Flag-Vangl1/Vector, Vector/Fzd7-HA, or Flag-Vangl1/Fzd7-HA in the GBM cell lines U251 and LN229 and assessed Vangl phosphorylation. We found that overexpression of Vangl1 and Fzd7 induced phosphorylation of Vangl compared to vector control or individually overexpressed proteins (Fig. 5D-E). This observation suggests a critical role for Vangl1 and Fzd7 in mediating downstream pathway activation in GBM cells.

To assess whether Vangl1/Fzd7 interactions are critical in mediating GBM cell motility, we employed the iDimerize Inducible Heterodimer System[32], to induce a constitutive interaction between Vangl1 and Fzd7 with the small molecule A/C Heterodimerizer (A/C). We stably co-overexpressed DmrC-Flag-Vangl1 and Fzd7-HA-DmrA (iDimer-VF) via lentiviral transduction into GBM cell lines to yield iDimer-VF-expressing U251 and LN229 cells and treated with A/C to induce dimerization (Fig. 5F). Increased cell migration was observed in GBMiDimer-VF cell lines upon treatment with A/C in a scratch migration assay (Fig. 5G-H). Notably, treatment with A/C in GBMiDimer cell lines (expressing DmrC-empty vector/empty vector-DmrA), GBMiDimer-V cell lines (expressing DmrC-Flag-Vangl1/empty vector-DmrA), or GBMiDimer-F cell lines (expressing DmrC-empty vector/Fzd7-HA-DmrA), did not result in an increase in cell motility (Supplementary Fig. 11A-F). Together, our data support a model where Vangl1 and Fzd7 interact endogenously and within cellular protrusions in migratory GBM cells, and this interaction may be critical to driving downstream outcomes in GBM tumors including cell migration.

3.6 Loss of Fzd7 impacts GBM growth in vivo and extends overall survival

Our *in vitro* and *ex vivo* findings suggest a mechanism by which Wnt/PCP components Vangl1 and Fzd7 contribute to the aggressive properties of GBM tumors. To assess if these observations are recapitulated *in vivo*, we asked whether perturbation of Wnt/PCP signaling impacts tumor growth and aggressiveness *in vivo.* To test this, we employed an intracranial xenograft model of GBM where we engrafted 10,000 luciferase-GFP-tagged U251 cells stably expressing shControl, shFzd7-1, or shFzd7-2 into NOD SCID mice. Tumor initiation and growth were monitored throughout the study via *in vivo* bioluminescence imaging. Mice were sacrificed upon display of moribund behavior or at 120 days after first tumor observation, and tissues were taken for histopathological analysis (Fig. 6A). Suppression of *FZD7* results in a significantly slower tumor growth rate, as observed by differences

in bioluminescence signal over time (Fig. 6B-C, Supplementary Fig. S12A). Differences in tumor size were also observed by MRI (Fig. 6D). Importantly, suppression of *FZD7* has a significant impact on tumor latency, where initiation of *FZD7* knockdown tumors occurs much later than control tumors (Fig. 6E), ultimately extending overall survival for mice bearing tumors with depleted *FZD7* expression (Fig. 6F). Decreased expression of *FZD7* in knockdown tumors was confirmed by immunohistochemical staining of Fzd7 (Supplementary Fig. S12B).

By histological analysis, U251-luciferase-GFP tumors displayed similar characteristics to that of human glioblastomas, including pleiomorphic morphology, pseudo-palisading necrosis, vascular proliferation, and mitosis[71-74]. Tumors depleted of *FZD7* displayed much slower growth than control tumors. However, because mice were not sacrificed at the same timepoint the tumor sizes at endpoint were comparable, with *FZD7* knockdown tumors occasionally being slightly smaller (Fig. 6G). Because transplanted cells express GFP, brain sections were stained with GFP to allow for more contrast between tumor and normal tissue (Fig. 6H) and to assess differences in invasion between the control and Fzd7 knockdown tumors. Unfortunately, the large tumor sizes at endpoint made it difficult to accurately assess differences in invasion because clear tumor borders were lacking. Additionally, loss of *FZD7* appeared to reduce cell proliferation as observed by differences in Ki67-positivity but did not completely pass our threshold for statistical significance for both shRNA knockdowns (Supplementary Fig. S12C-D). Because Fzd7 is a shared component with canonical Wnt signaling[75], we sought to rule out whether the effects on GBM proliferation were canonical Wnt signaling-dependent by assessing the phosphorylation status of β-catenin, a core component of the pathway[76]. We observed no appreciable differences in β-catenin phosphorylation in U251 cells depleted of *FZD7* by western blotting (Supplementary Fig. S12E-F), suggesting that the observed effects on proliferation upon *FZD7* loss are likely noncanonical Wnt signaling-specific. Together, these results indicate that Fzd7 is an important driver of the aggressive properties of GBM tumors *in vivo*.

4. Discussion

Increasing evidence supports a role for Wnt/PCP signaling in mediating malignant behavior across diverse solid tumor types[13,14]. We previously reported that Wnt/PCP components *WNT5A, VANGL1,* and *FZD7* transcripts are elevated in GBM tumors regardless of subtype, and correlate with poorer patient survival[17]. Further, we identified the E3 ubiquitin ligase Nrdp1 as a novel negative regulator of Wnt/PCP signaling and found that restoration of *NRDP1* expression significantly reduced GBM cell motility[17]. We demonstrated that core Wnt/PCP components are necessary for Nrdp1 to impact GBM malignancy, but their role in GBM malignancy and the underlying mechanisms remain poorly defined, creating an opportunity to identify targetable contributors. Therefore, we aimed to characterize the role of key Wnt/PCP components in GBM hyperproliferation and invasiveness *in vitro* and *in vivo.*

While Vangl1 and Fzd7 have been reported to mediate cell motility and proliferation in several other cancer types[39-41,54,77], their contribution to GBM malignancy remain largely

unexplored despite their elevated expression levels[17,78]. Here, our data point to a novel molecular model whereby core Wnt/PCP components Vangl1 and Fzd7 localize and interact at the leading edge of migratory GBM cells to engage downstream effectors, such as Dvl and Rac1, to regulate actin cytoskeletal rearrangements critical to the aggressive properties of GBM tumors (Fig. 7). Using a diverse panel of GBM cell lines, we found that cellular proliferation and motility are reduced upon loss of *VANGL1 or FZD7 in vitro.* Further, we employed both a 3D collagen matrix assay and an *ex vivo* brain slice assay and observed a significant reduction in GBM cell invasion when *VANGL1* or *FZD7* are knocked down, indicating a critical role for Wnt/PCP components in regulating GBM aggressiveness.

Rho GTPases are important master regulators of cytoskeletal rearrangements and actin dynamics, mediating biological processes such as cell motility and proliferation[50], and have long been implicated as downstream regulators of Wnt/PCP-mediated polarity and motility[17,51,52,79]. Rac1 and RhoA have been previously reported to regulate GBM invasiveness. In one report, invading GBM cells displayed elevated Rac1 and Cdc42 activity, but lower RhoA activity[55], consistent with reports that Rac1 and RhoA can be antagonistic[80]. In our study, we employed intramolecular FRET biosensors to assess temporal and spatial changes in GTPase activity[27] upon perturbation of Wnt/PCP components. We demonstrate that Rac1 activity increases over ten hours of migration in control cells, and that loss of *VANGL1* or *FZD7* significantly dampens this effect and reduces basal Rac1 activity levels. In contrast, while loss of *VANGL1* or *FZD7* reduces RhoA activity, we observed a general decrease in RhoA GTPase activity with motility over time. We also found that Rac1 activity is localized at the leading edge of migratory GBM cells, suggesting that recruitment of Rac1 to cellular protrusions is critical for GBM cell motility. Further, our findings that loss of *VANGL1* or *FZD7* impair leading-edge actin dynamics strongly suggests that impaired cell motility in GBM cells with ablated *VANGL1* or *FZD7* expression results from dysregulated cytoskeletal rearrangements. Collectively, our observations that Vangl1 and Fzd7 influence both Rac1 and RhoA activity and mediate actin dynamics indicate that Wnt/PCP is an important regulator of both cellular protrusion and retraction to drive cell motility.

Proper localization of Wnt/PCP components is critical for pathway function, yet information on component localization in migratory cells comes primarily from studies in breast cancer cells where the model remains disputed[39,40]. This stems largely from conflicting reports on the localization pattern of Vangl in migrating breast cancer cells, where one study reported Vangl to be localized at the leading edge of lamellipodia[39], while another reported Vangl localization at base of the cellular protrusions but absent from the protrusive front[40]. Here, our studies reveal that Vangl1 and Fzd7 co-localize within actin-rich protrusions in migratory GBM cells, and that Dvl2 is localized both within the cytoplasm and at the plasma membrane, consistent with reports that both Vangl and Fzd are able to recruit Dvl to the membrane[59,61]. Further, we demonstrate through co-immunoprecipitation and proximity ligation assays that Vang1 and Fzd7 interact endogenously within protrusions from single migratory GBM cells. Finally, our experiments using the iDimerize Inducible Heterodimer System[32] demonstrate that interaction of Vangl1 with Fzd7 increases GBM cell migration. Together, these observations suggest that asymmetric localization of opposing complexes is not necessary in migratory GBM cells and suggest that the release of these

components from constraints imposed by epithelial planar polarity mechanisms could be important in the engagement of downstream effectors that drive cell motility. Moreover, an intramembrane Vangl1/Fzd7 complex may be imperative for the recruitment and activation of downstream effectors such as Dvl and Rho GTPases, creating a functional signalosome critical to mediating biological outcomes.

Finally, we report a critical role for Fzd7 in mediating GBM malignancy *in vivo* using an intracranial xenograft model of GBM. Loss of *FZD7* expression in U251 cells engrafted into mouse brains significantly affected tumor growth and latency and extended overall survival. These findings are consistent with, and significantly improve upon, previous reports that overexpression of *FZD7* increases GBM proliferation and decreases survival when xenografted into flanks of immunocompromised mice[81]. The multifaceted contribution of Fzd7 to GBM malignancy *in vivo* suggests that this receptor could be a viable target for successful clinical intervention. Indeed, in recent years Fzd7 antagonists have been developed for use as anticancer therapeutics in other tumor types[82], and have shown some therapeutic efficacy in preclinical models and early phase clinical trials[83,84]. Of note, several studies investigating microRNAs whose targets include Fzd7 have shown significant reduction of GBM cellular proliferation, motility, and tumor growth[85-87], suggesting that targeting of Fzd7 could be beneficial in GBM tumors.

Overall, this study defines a critical role for core Wnt/PCP components Vangl1 and Fzd7 in driving the aggressive properties of GBM tumors. We propose a mechanism by which Vangl1 and Fzd7 interact at the leading edge of cellular protrusions where they can engage downstream effectors including Dvl and Rho GTPases to yield alterations in cytoskeletal rearrangements and actin dynamics to drive GBM cell motility. Further, our findings implicate Fzd7 as a significant contributor to GBM malignancy *in vivo* and suggest that targeting of Fzd7 could provide improved clinical benefit for patients diagnosed with the disease.

Supplementary Material

Refer to Web version on PubMed Central for supplementary material.

Acknowledgements

Abbreviations

GBM	glioblastoma multiforme
Wnt/PCP	Wnt/Planar cell polarity
Fzd	Frizzled
Dvl	Dishevelled

PLA	proximity ligation assay
A/C	A/C Heterodimerizer

6. References

1. Bianco J, Bastiancich C, Jankovski A, des Rieux A, Préat V & Danhier F On glioblastoma and the search for a cure: where do we stand? Cell Mol Life Sci 74, 2451–2466 (2017). 10.1007/s00018-017-2483-3 [PubMed: 28210785]

2. Alifieris C & Trafalis DT Glioblastoma multiforme: Pathogenesis and treatment. Pharmacol Ther 152, 63–82 (2015). 10.1016/j.pharmthera.2015.05.005 [PubMed: 25944528]

3. Kim Y. Regulation of Cell Proliferation and Migration in Glioblastoma: New Therapeutic Approach. Frontiers in oncology 3 (2013). 10.3389/fonc.2013.00053

4. Osuka S & Van Meir EG Overcoming therapeutic resistance in glioblastoma: the way forward. The Journal of clinical investigation 127, 415–426 (2017). 10.1172/jci89587 [PubMed: 28145904]

5. Eskilsson E, Røsland GV, Solecki G, Wang Q, Harter PN, Graziani G et al. EGFR heterogeneity and implications for therapeutic intervention in glioblastoma. Neuro-Oncology 20, 743–752 (2017). 10.1093/neuonc/nox191

6. Hoelzinger DB, Demuth T & Berens ME Autocrine Factors That Sustain Glioma Invasion and Paracrine Biology in the Brain Microenvironment. JNCI: Journal of the National Cancer Institute 99, 1583–1593 (2007). 10.1093/jnci/djm187 [PubMed: 17971532]

7. Koul D. PTEN Signaling pathways in glioblastoma. Cancer Biology & Therapy 7, 1321–1325 (2008). 10.4161/cbt.7.9.6954 [PubMed: 18836294]

8. Zanders ED, Svensson F & Bailey DS Therapy for glioblastoma: is it working? Drug Discovery Today 24, 1193–1201 (2019). 10.1016/j.drudis.2019.03.008 [PubMed: 30878561]

9. Cihoric N, Tsikkinis A, Minniti G, Lagerwaard FJ, Herrlinger U, Mathier E et al. Current status and perspectives of interventional clinical trials for glioblastoma – analysis of ClinicalTrials.gov. Radiation Oncology 12, 1 (2017). 10.1186/s13014-016-0740-5 [PubMed: 28049492]

10. Taylor OG, Brzozowski JS & Skelding KA Glioblastoma Multiforme: An Overview of Emerging Therapeutic Targets. Frontiers in oncology 9 (2019). 10.3389/fonc.2019.00963

11. Devenport D. The cell biology of planar cell polarity. Journal of Cell Biology 207, 171–179 (2014). 10.1083/jcb.201408039 [PubMed: 25349257]

12. Butler MT & Wallingford JB Planar cell polarity in development and disease. Nat Rev Mol Cell Biol 18, 375–388 (2017). 10.1038/nrm.2017.11 [PubMed: 28293032]

13. Hatakeyama J, Wald JH, Printsev I, Ho HY & Carraway KL 3rd. Vangl1 and Vangl2: planar cell polarity components with a developing role in cancer. Endocr Relat Cancer 21, R345–356 (2014). 10.1530/erc-14-0141 [PubMed: 24981109]

14. VanderVorst K, Hatakeyama J, Berg A, Lee H & Carraway KL 3rd. Cellular and molecular mechanisms underlying planar cell polarity pathway contributions to cancer malignancy. Seminars in cell & developmental biology 81, 78–87 (2018). 10.1016/j.semcdb.2017.09.026 [PubMed: 29107170]

15. Dreyer CA, VanderVorst K & Carraway KL Vangl as a Master Scaffold for Wnt/Planar Cell Polarity Signaling in Development and Disease. Frontiers in Cell and Developmental Biology 10 (2022). 10.3389/fcell.2022.887100

16. VanderVorst K, Dreyer CA, Hatakeyama J, Bell GRR, Berg AL, Hernandez M et al. Wnt/PCP signaling mediates breast cancer metastasis by promoting pro-invasive protrusion formation in collectively motile leader cells. bioRxiv, 2022.2001.2007.475316 (2022). 10.1101/2022.01.07.475316

17. Wald JH, Hatakeyama J, Printsev I, Cuevas A, Fry WHD, Saldana MJ et al. Suppression of planar cell polarity signaling and migration in glioblastoma by Nrdp1-mediated Dvl polyubiquitination. Oncogene 36, 5158–5167 (2017). 10.1038/onc.2017.126 [PubMed: 28481871]

18. Uphoff CC & Drexler HG Comparative PCR analysis for detection of mycoplasma infections in continuous cell lines. In Vitro Cell Dev Biol Anim 38, 79–85 (2002). 10.1290/1071-2690(2002)038<0079:Cpafdo>2.0.Co;2 [PubMed: 11928999]

19. Uphoff CC & Drexler HG Detecting mycoplasma contamination in cell cultures by polymerase chain reaction. Methods Mol Biol 731, 93–103 (2011). 10.1007/978-1-61779-080-5_8 [PubMed: 21516400]

20. Sarbassov DD, Guertin DA, Ali SM & Sabatini DM Phosphorylation and regulation of Akt/PKB by the rictor-mTOR complex. Science (New York, N.Y.) 307, 1098–1101 (2005). 10.1126/science.1106148 [PubMed: 15718470]

21. Smith MA, Blankman E, Deakin NO, Hoffman LM, Jensen CC, Turner CE et al. LIM domains target actin regulators paxillin and zyxin to sites of stress fiber strain. PloS one 8, e69378 (2013). 10.1371/journal.pone.0069378 [PubMed: 23990882]

22. Beegle J, Lakatos K, Kalomoiris S, Stewart H, Isseroff RR, Nolta JA et al. Hypoxic preconditioning of mesenchymal stromal cells induces metabolic changes, enhances survival, and promotes cell retention in vivo. Stem Cells 33, 1818–1828 (2015). 10.1002/stem.1976 [PubMed: 25702874]

23. Eisemann T, Costa B, Strelau J, Mittelbronn M, Angel P & Peterziel H An advanced glioma cell invasion assay based on organotypic brain slice cultures. BMC Cancer 18, 103 (2018). 10.1186/s12885-018-4007-4 [PubMed: 29378533]

24. Ke M-T, Fujimoto S & Imai T SeeDB: a simple and morphology-preserving optical clearing agent for neuronal circuit reconstruction. Nature Neuroscience 16, 1154–1161 (2013). 10.1038/nn.3447 [PubMed: 23792946]

25. Nguyen-Ngoc KV, Cheung KJ, Brenot A, Shamir ER, Gray RS, Hines WC et al. ECM microenvironment regulates collective migration and local dissemination in normal and malignant mammary epithelium. Proceedings of the National Academy of Sciences of the United States of America 109, E2595–2604 (2012). 10.1073/pnas.1212834109 [PubMed: 22923691]

26. Itoh RE, Kurokawa K, Ohba Y, Yoshizaki H, Mochizuki N & Matsuda M Activation of rac and cdc42 video imaged by fluorescent resonance energy transfer-based single-molecule probes in the membrane of living cells. Molecular and cellular biology 22, 6582–6591 (2002). 10.1128/mcb.22.18.6582-6591.2002 [PubMed: 12192056]

27. Komatsu N, Aoki K, Yamada M, Yukinaga H, Fujita Y, Kamioka Y et al. Development of an optimized backbone of FRET biosensors for kinases and GTPases. Molecular biology of the cell 22, 4647–4656 (2011). 10.1091/mbc.e11-01-0072 [PubMed: 21976697]

28. Bell GRR, Rincón E, Akdo an E & Collins SR Optogenetic control of receptors reveals distinct roles for actin- and Cdc42-dependent negative signals in chemotactic signal processing. Nature Communications 12, 6148 (2021). 10.1038/s41467-021-26371-z

29. Yang HW, Collins SR & Meyer T Locally excitable Cdc42 signals steer cells during chemotaxis. Nature cell biology 18, 191–201 (2016). 10.1038/ncb3292 [PubMed: 26689677]

30. Printsev I, Yen L, Sweeney C & Carraway KL Oligomerization of the Nrdp1 E3 Ubiquitin Ligase Is Necessary for Efficient Autoubiquitination but Not ErbB3 Ubiquitination*. Journal of Biological Chemistry 289, 8570–8578 (2014). 10.1074/jbc.M113.527036 [PubMed: 24519943]

31. Hatakeyama J, Wald JH, Rafidi H, Cuevas A, Sweeney C & Carraway KL 3rd. The ER structural protein Rtn4A stabilizes and enhances signaling through the receptor tyrosine kinase ErbB3. Science signaling 9, ra65 (2016). 10.1126/scisignal.aaf1604 [PubMed: 27353365]

32. Rivera VM, Berk L & Clackson T Dimerizer-mediated regulation of gene expression in vivo. Cold Spring Harb Protoc 2012, 821–824 (2012). 10.1101/pdb.prot070144 [PubMed: 22753599]

33. Rowson-Hodel AR, Manjarin R, Trott JF, Cardiff RD, Borowsky AD & Hovey RC Neoplastic transformation of porcine mammary epithelial cells in vitro and tumor formation in vivo. BMC Cancer 15, 562 (2015). 10.1186/s12885-015-1572-7 [PubMed: 26228788]

34. Rowson-Hodel AR, Wald JH, Hatakeyama J, O'Neal WK, Stonebraker JR, VanderVorst K et al. Membrane Mucin Muc4 promotes blood cell association with tumor cells and mediates efficient metastasis in a mouse model of breast cancer. Oncogene 37, 197–207 (2018). 10.1038/onc.2017.327 [PubMed: 28892049]

35. Giannini C, Sarkaria JN, Saito A, Uhm JH, Galanis E, Carlson BL et al. Patient tumor EGFR and PDGFRA gene amplifications retained in an invasive intracranial xenograft model of glioblastoma multiforme. Neuro Oncol 7, 164–176 (2005). 10.1215/s1152851704000821 [PubMed: 15831234]

36. Candolfi M, Curtin JF, Nichols WS, Muhammad AG, King GD, Pluhar GE et al. Intracranial glioblastoma models in preclinical neuro-oncology: neuropathological characterization and tumor progression. J Neurooncol 85, 133–148 (2007). 10.1007/s11060-007-9400-9 [PubMed: 17874037]

37. Zhao Y, Xiao A, diPierro CG, Carpenter JE, Abdel-Fattah R, Redpath GT et al. An extensive invasive intracranial human glioblastoma xenograft model: role of high level matrix metalloproteinase 9. Am J Pathol 176, 3032–3049 (2010). 10.2353/ajpath.2010.090571 [PubMed: 20413683]

38. Hlavaty J, Jandl G, Liszt M, Petznek H, König-Schuster M, Sedlak J et al. Comparative evaluation of preclinical in vivo models for the assessment of replicating retroviral vectors for the treatment of glioblastoma. Journal of Neuro-Oncology 102, 59–69 (2011). 10.1007/s11060-010-0295-5 [PubMed: 20623247]

39. Anastas JN, Biechele TL, Robitaille M, Muster J, Allison KH, Angers S et al. A protein complex of SCRIB, NOS1AP and VANGL1 regulates cell polarity and migration, and is associated with breast cancer progression. Oncogene 31, 3696–3708 (2012). 10.1038/onc.2011.528 [PubMed: 22179838]

40. Luga V, Zhang L, Viloria-Petit Alicia M., Ogunjimi Abiodun A., Inanlou Mohammad R., Chiu E et al. Exosomes Mediate Stromal Mobilization of Autocrine Wnt-PCP Signaling in Breast Cancer Cell Migration. Cell 151, 1542–1556 (2012). 10.1016/j.cell.2012.11.024 [PubMed: 23260141]

41. Daulat Avais M., Bertucci F, Audebert S, Sergé A, Finetti P, Josselin E et al. PRICKLE1 Contributes to Cancer Cell Dissemination through Its Interaction with mTORC2. Developmental cell 37, 311–325 (2016). 10.1016/j.devcel.2016.04.011 [PubMed: 27184734]

42. Venkataramani V, Yang Y, Schubert MC, Reyhan E, Tetzlaff SK, Wißmann N et al. Glioblastoma hijacks neuronal mechanisms for brain invasion. Cell 185, 2899–2917.e2831 (2022). 10.1016/j.cell.2022.06.054 [PubMed: 35914528]

43. Vollmann-Zwerenz A, Leidgens V, Feliciello G, Klein CA & Hau P Tumor Cell Invasion in Glioblastoma. Int J Mol Sci 21 (2020). 10.3390/ijms21061932

44. Friedl P, Locker J, Sahai E & Segall JE Classifying collective cancer cell invasion. Nature cell biology 14, 777–783 (2012). 10.1038/ncb2548 [PubMed: 22854810]

45. Cuddapah VA, Robel S, Watkins S & Sontheimer H A neurocentric perspective on glioma invasion. Nature Reviews Neuroscience 15, 455–465 (2014). 10.1038/nrn3765 [PubMed: 24946761]

46. Seifert JRK & Mlodzik M Frizzled/PCP signalling: a conserved mechanism regulating cell polarity and directed motility. Nature Reviews Genetics 8, 126–138 (2007). 10.1038/nrg2042

47. Krneta-Stankic V, Corkins ME, Paulucci-Holthauzen A, Kloc M, Gladden AB & Miller RK The Wnt/PCP formin Daam1 drives cell-cell adhesion during nephron development. Cell Reports 36, 109340 (2021). 10.1016/j.celrep.2021.109340 [PubMed: 34233186]

48. Walsh FS & Doherty P Neural cell adhesion molecules of the immunoglobulin superfamily: Role in axon growth and guidance. Annual Review of Cell and Developmental Biology 13, 425–456 (1997).

49. Ridley AJ, Schwartz MA, Burridge K, Firtel RA, Ginsberg MH, Borisy G et al. Cell Migration: Integrating Signals from Front to Back. Science (New York, N.Y.) 302, 1704–1709 (2003). doi:10.1126/science.1092053 [PubMed: 14657486]

50. Etienne-Manneville S & Hall A Rho GTPases in cell biology. Nature 420, 629–635 (2002). 10.1038/nature01148 [PubMed: 12478284]

51. Habas R, Dawid IB & He X Coactivation of Rac and Rho by Wnt/Frizzled signaling is required for vertebrate gastrulation. Genes Dev 17, 295–309 (2003). 10.1101/gad.1022203 [PubMed: 12533515]

52. Habas R, Kato Y & He X Wnt/Frizzled activation of Rho regulates vertebrate gastrulation and requires a novel Formin homology protein Daam1. Cell 107, 843–854 (2001). 10.1016/s0092-8674(01)00614-6 [PubMed: 11779461]

53. Kurayoshi M, Oue N, Yamamoto H, Kishida M, Inoue A, Asahara T et al. Expression of Wnt-5a Is Correlated with Aggressiveness of Gastric Cancer by Stimulating Cell Migration and Invasion. Cancer research 66, 10439–10448 (2006). 10.1158/0008-5472.Can-06-2359 [PubMed: 17079465]

54. Asad M, Wong MK, Tan TZ, Choolani M, Low J, Mori S et al. FZD7 drives in vitro aggressiveness in Stem-A subtype of ovarian cancer via regulation of non-canonical Wnt/PCP pathway. Cell death & disease 5, e1346 (2014). 10.1038/cddis.2014.302 [PubMed: 25032869]

55. Hirata E, Yukinaga H, Kamioka Y, Arakawa Y, Miyamoto S, Okada T et al. In vivo fluorescence resonance energy transfer imaging reveals differential activation of Rho-family GTPases in glioblastoma cell invasion. Journal of cell science 125, 858–868 (2012). 10.1242/jcs.089995 [PubMed: 22399802]

56. Riedl J, Crevenna AH, Kessenbrock K, Yu JH, Neukirchen D, Bista M et al. Lifeact: a versatile marker to visualize F-actin. Nat Methods 5, 605–607 (2008). 10.1038/nmeth.1220 [PubMed: 18536722]

57. Lauffenburger DA & Horwitz AF Cell migration: a physically integrated molecular process. Cell 84, 359–369 (1996). 10.1016/s0092-8674(00)81280-5 [PubMed: 8608589]

58. Tree DRP, Shulman JM, Rousset R, Scott MP, Gubb D & Axelrod JD Prickle Mediates Feedback Amplification to Generate Asymmetric Planar Cell Polarity Signaling. Cell 109, 371–381 (2002). https://doi.org:10.1016/S0092-8674(02)00715-8 [PubMed: 12015986]

59. Bastock R, Strutt H & Strutt D Strabismus is asymmetrically localised and binds to Prickle and Dishevelled during Drosophila planar polarity patterning. Development 130, 3007–3014 (2003). 10.1242/dev.00526 [PubMed: 12756182]

60. Strutt DI Asymmetric Localization of Frizzled and the Establishment of Cell Polarity in the Drosophila Wing. Molecular Cell 7, 367–375 (2001). https://doi.org:10.1016/S1097-2765(01)00184-8 [PubMed: 11239465]

61. Axelrod JD Unipolar membrane association of Dishevelled mediates Frizzled planar cell polarity signaling. Genes Dev 15, 1182–1187 (2001). 10.1101/gad.890501 [PubMed: 11358862]

62. Jenny A, Darken RS, Wilson PA & Mlodzik M Prickle and Strabismus form a functional complex to generate a correct axis during planar cell polarity signaling. The EMBO Journal 22, 4409–4420 (2003). 10.1093/emboj/cdg424 [PubMed: 12941693]

63. Strutt H & Strutt D Asymmetric localisation of planar polarity proteins: Mechanisms and consequences. Seminars in cell & developmental biology 20, 957–963 (2009). 10.1016/j.semcdb.2009.03.006 [PubMed: 19751618]

64. Cho B, Pierre-Louis G, Sagner A, Eaton S & Axelrod JD Clustering and Negative Feedback by Endocytosis in Planar Cell Polarity Signaling Is Modulated by Ubiquitinylation of Prickle. PLOS Genetics 11, e1005259 (2015). 10.1371/journal.pgen.1005259 [PubMed: 25996914]

65. Das G, Jenny A, Klein TJ, Eaton S & Mlodzik M Diego interacts with Prickle and Strabismus/Van Gogh to localize planar cell polarity complexes. Development 131, 4467–4476 (2004). 10.1242/dev.01317 [PubMed: 15306567]

66. Montcouquiol M, Sans N, Huss D, Kach J, Dickman JD, Forge A et al. Asymmetric Localization of Vangl2 and Fz3 Indicate Novel Mechanisms for Planar Cell Polarity in Mammals. The Journal of Neuroscience 26, 5265–5275 (2006). 10.1523/jneurosci.4680-05.2006 [PubMed: 16687519]

67. Gao B, Song H, Bishop K, Elliot G, Garrett L, English MA et al. Wnt Signaling Gradients Establish Planar Cell Polarity by Inducing Vangl2 Phosphorylation through Ror2. Developmental cell 20, 163–176 (2011). 10.1016/j.devcel.2011.01.001 [PubMed: 21316585]

68. Kelly LK, Wu J, Yanfeng WA & Mlodzik M Frizzled-Induced Van Gogh Phosphorylation by CK1ε Promotes Asymmetric Localization of Core PCP Factors in Drosophila. Cell Reports 16, 344–356 (2016). 10.1016/j.celrep.2016.06.010 [PubMed: 27346358]

69. Yang W, Garrett L, Feng D, Elliott G, Liu X, Wang N et al. Wnt-induced Vangl2 phosphorylation is dose-dependently required for planar cell polarity in mammalian development. Cell Research 27, 1466–1484 (2017). 10.1038/cr.2017.127 [PubMed: 29056748]

70. Gao B, Ajima R, Yang W, Li C, Song H, Anderson MJ et al. Coordinated directional outgrowth and pattern formation by integration of Wnt5a and Fgf signaling in planar cell polarity. Development 145 (2018). 10.1242/dev.163824

71. Rong Y, Durden DL, Van Meir EG & Brat DJ 'Pseudopalisading' Necrosis in Glioblastoma: A Familiar Morphologic Feature That Links Vascular Pathology, Hypoxia, and Angiogenesis. Journal of Neuropathology & Experimental Neurology 65, 529–539 (2006). 10.1097/00005072-200606000-00001 [PubMed: 16783163]

72. Brat DJ, Castellano-Sanchez AA, Hunter SB, Pecot M, Cohen C, Hammond EH et al. Pseudopalisades in Glioblastoma Are Hypoxic, Express Extracellular Matrix Proteases, and Are Formed by an Actively Migrating Cell Population. Cancer research 64, 920–927 (2004). 10.1158/0008-5472.Can-03-2073 [PubMed: 14871821]

73. Fischer I, Gagner JP, Law M, Newcomb EW & Zagzag D Angiogenesis in gliomas: biology and molecular pathophysiology. Brain Pathol 15, 297–310 (2005). 10.1111/j.1750-3639.2005.tb00115.x [PubMed: 16389942]

74. D'Alessio A, Proietti G, Sica G & Scicchitano BM Pathological and Molecular Features of Glioblastoma and Its Peritumoral Tissue. Cancers 11 (2019). 10.3390/cancers11040469

75. Li G, Su Q, Liu H, Wang D, Zhang W, Lu Z et al. Frizzled7 Promotes Epithelial-to-mesenchymal Transition and Stemness Via Activating Canonical Wnt/β-catenin Pathway in Gastric Cancer. Int J Biol Sci 14, 280–293 (2018). 10.7150/ijbs.23756 [PubMed: 29559846]

76. van Amerongen R. Alternative Wnt pathways and receptors. Cold Spring Harb Perspect Biol 4 (2012). 10.1101/cshperspect.a007914

77. Wang L, Wang J, Yin X, Guan X, Li Y, Xin C et al. GIPC2 interacts with Fzd7 to promote prostate cancer metastasis by activating WNT signaling. Oncogene 41, 2609–2623 (2022). 10.1038/s41388-022-02255-4 [PubMed: 35347223]

78. Sun L, Hui AM, Su Q, Vortmeyer A, Kotliarov Y, Pastorino S et al. Neuronal and glioma-derived stem cell factor induces angiogenesis within the brain. Cancer cell 9, 287–300 (2006). 10.1016/j.ccr.2006.03.003 [PubMed: 16616334]

79. Zhang L, Luga V, Armitage SK, Musiol M, Won A, Yip CM et al. A lateral signalling pathway coordinates shape volatility during cell migration. Nature Communications 7, 11714 (2016). 10.1038/ncomms11714

80. Parri M & Chiarugi P Rac and Rho GTPases in cancer cell motility control. Cell Communication and Signaling 8, 23 (2010). 10.1186/1478-811X-8-23 [PubMed: 20822528]

81. Qiu X, Jiao J, Li Y & Tian T Overexpression of FZD7 promotes glioma cell proliferation by upregulating TAZ. Oncotarget 7, 85987–85999 (2016). 10.18632/oncotarget.13292 [PubMed: 27852064]

82. Larasati Y, Boudou C, Koval A & Katanaev VL Unlocking the Wnt pathway: Therapeutic potential of selective targeting FZD7 in cancer. Drug Discovery Today 27, 777–792 (2022). 10.1016/j.drudis.2021.12.008 [PubMed: 34915171]

83. Do M, Wu CCN, Sonavane PR, Juarez EF, Adams SR, Ross J et al. A FZD7-specific Antibody–Drug Conjugate Induces Ovarian Tumor Regression in Preclinical Models. Molecular Cancer Therapeutics 21, 113–124 (2022). 10.1158/1535-7163.Mct-21-0548 [PubMed: 34667113]

84. Davis SL, Cardin DB, Shahda S, Lenz H-J, Dotan E, O'Neil BH et al. A phase 1b dose escalation study of Wnt pathway inhibitor vantictumab in combination with nab-paclitaxel and gemcitabine in patients with previously untreated metastatic pancreatic cancer. Investigational New Drugs 38, 821–830 (2020). 10.1007/s10637-019-00824-1 [PubMed: 31338636]

85. Zhou F, Cao W, Xu R, Zhang J, Yu T, Xu X et al. MicroRNA-206 attenuates glioma cell proliferation, migration, and invasion by blocking the WNT/β-catenin pathway via direct targeting of Frizzled 7 mRNA. Am J Transl Res 11, 4584–4601 (2019). [PubMed: 31396362]

86. Cheng ZX, Song YX, Wang ZY, Wang Y & Dong Y miR-144-3p serves as a tumor suppressor by targeting FZD7 and predicts the prognosis of human glioblastoma. Eur Rev Med Pharmacol Sci 21, 4079–4086 (2017). [PubMed: 29028093]

87. Liu Q, Guan Y, Li Z, Wang Y, Liu Y, Cui R et al. miR-504 suppresses mesenchymal phenotype of glioblastoma by directly targeting the FZD7-mediated Wnt–β-catenin pathway. Journal of Experimental & Clinical Cancer Research 38, 358 (2019). 10.1186/s13046-019-1370-1 [PubMed: 31419987]
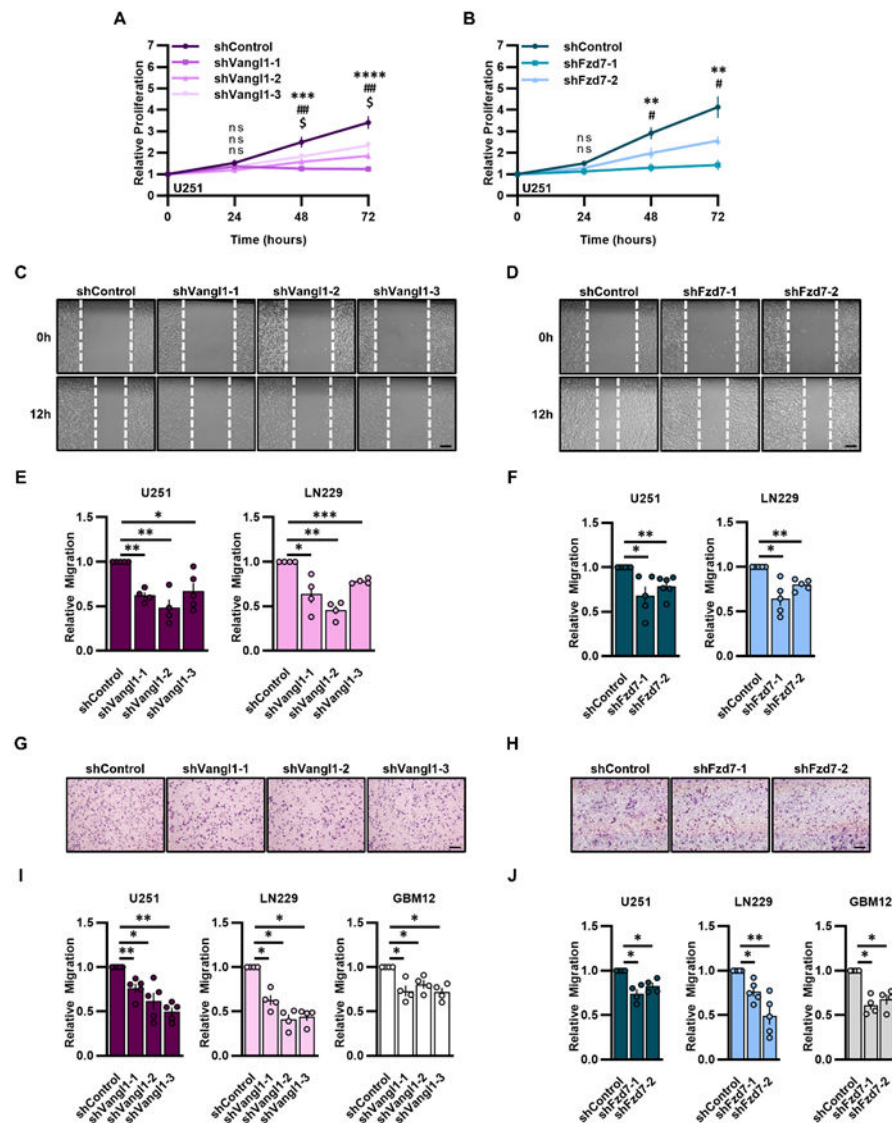
Figure 1. Vangl1 and Fzd7 promote GBM growth and aggressiveness.
A-B Relative proliferation of U251 cells stably expressing shControl, shVangl1-1, shVangl1-2, or shVangl1-3 at 24, 48, and 72 hours (t-test: 24 hours (*n*=9): *p*=0.4418, *p*=0.0887, and *p*=0.4551, 48 hours (*n*=9): *p*=0.0003, *p*=0.0065, and *p*=0.0403, 72 hours (*n*=6): *p*=4.99E-05, *p*=0.0011, and *p*=0.0175; ANOVA: 24 hours (*n*=9): *p*=0.7471, *p*=0.2439, and *p*=0.7396, 48 hours (*n*=9): *p*<0.0001, *p*=0.0015, and *p*=0.0235, 72 hours (*n*=6): *p*<0001, *p*=0.0002, and *p*=0.0059) **(A)** or shControl, shFzd7-1, or shFzd7-2 at 24, 48, and 72 hours (t-test: 24 hours (*n*=6): *p*=0.1370, and *p*=0.3600, 48 hours (*n*=6): *p*=0.0011, and 0.0376, 72 hours (*n*=6): *p*=0.0188, and *p*=0.0269; ANOVA: 24 hours (*n*=9): *p*=0.2450, and *p*=0.5780, 48 hours (*n*=9): *p*=0.0008, and *p*=0.0371, 72 hours (*n*=6): *p*=0.0001, and *p*=0.0120) **(B)**. **C-D** Representative images of migrating U251 cells stably expressing shControl, shVangl1-1, shVangl1-2, or shVangl1-3 **(C)** or shControl, shFzd7-1, or shFzd7-2 **(D)** at 0 and 12 hours in a scratch migration assay. Scale bar=200μm. **E-F** Quantification of the relative migration of U251 and LN229 cells stably expressing shControl, shVangl1-1, shVangl1-2, or shVangl1-3

(U251: n=4 or 5, t-test: p=0.0020, p=0.0115, and p=0.0223, ANOVA: p=0.0040, p=0.0003, and p=0.0072; LN229: n=4, t-test: p=0.0379, p=0.0016, and p=0.0005, ANOVA: p=0.0020, p<0.0001, and p=0.0465) **(E)** or shControl, shFzd7-1, or shFzd7-2 (U251: n=5 or 6, t-test: p=0.0335, and p=0.0057, ANOVA: p=0.0013, and p=0.0421; LN229: n=5, t-test: p=0.0118, and p=0.0017, ANOVA: p=0.0005, and p=0.0251) **(F)** in a 12-hour scratch migration assay. **G-H** Representative images of migrated U251 cells stably expressing shControl, shVangl1-1, shVangl1-2, or shVangl1-3 **(G)** or shControl, shFzd7-1, or shFzd7-2 **(H)** stained with Diff Stain in Boyden chambers. Scale bar=200μm. **I-J** Quantification of the relative migration of U251, LN229 and GBM12 cells stably expressing shControl, shVangl1-1, shVangl1-2, or shVangl1-3 (U251: n=5, t-test: p=0.0088, p=0.0145, and p=0.0004, ANOVA: p=0.0257, p=0.0007, and p<0.0001; LN229: n=4, t-test: p=0.0075, p=0.0019, and p=0.0013, ANOVA: p=0.0003, p<0.0001, and p<0.0001; GBM12: n=4, t-test: p=0.0209, p=0.0259, and p=0.0095, ANOVA: p=0.0031, p=0.0264, and p=0.0021) **(I)** or shControl, shFzd7-1, or shFzd7-2 (U251: n=4, t-test: p=0.0127, and p=0.0205, ANOVA: p=0.0012, and p=0.0136; LN229: n=5, t-test: p=0.0107, and p=0.0063, ANOVA: p=0.0407, and p=0.0002; GBM12: n=4; t-test: p=0.0051, and p=0.0111, ANOVA: p=0.0004, and p=0.0012) **(J)** in a Boyden chamber assay. Errors bars depict SEM. Statistical significance was calculated using an unpaired two-tailed t-test with Welch's correction or one-way ANOVA with multiple comparisons. * denotes statistical significance for sh1, # denotes statistical significance for sh2, and $ denotes statistical significance for sh3 **(A-B)**.
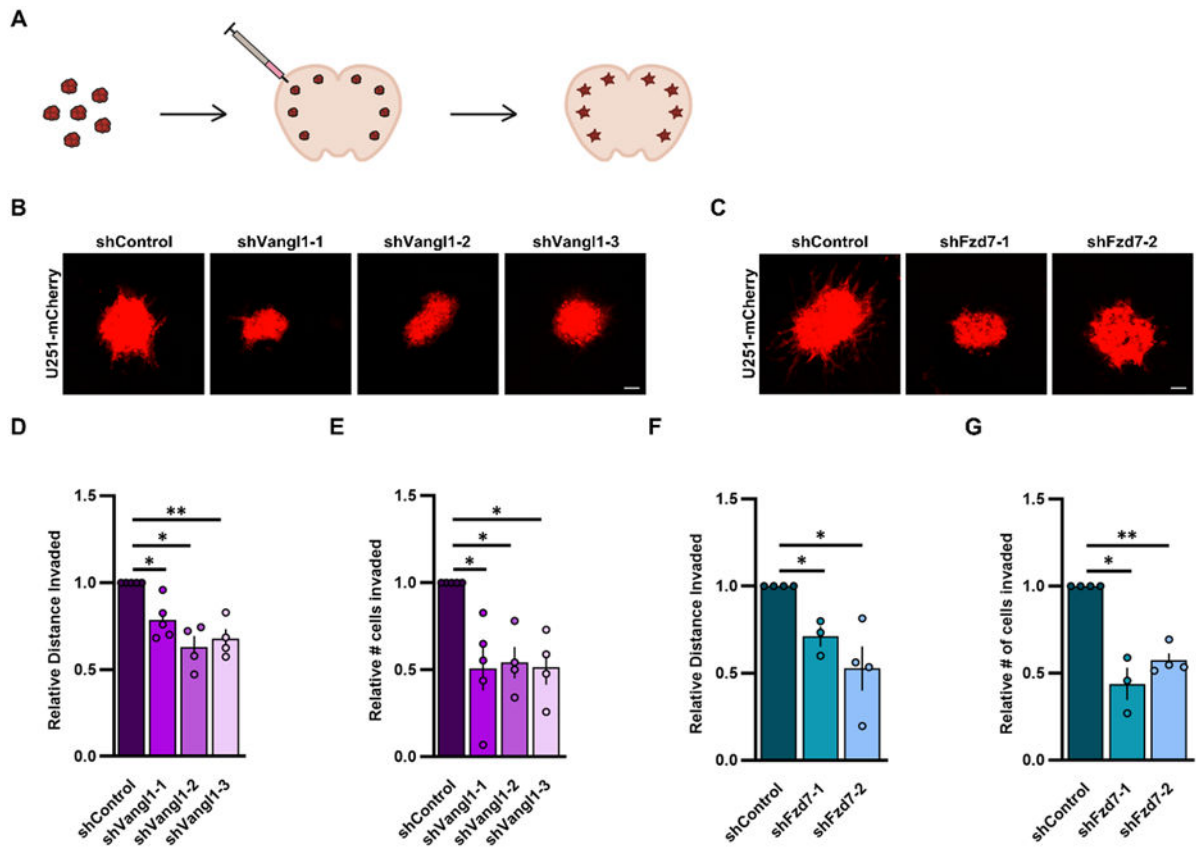
Figure 2. Vangl1 and Fzd7 promote GBM spheroid invasion *ex vivo*.
A Schematic depiction of the organotypic brain slice assay employed to assess GBM cell invasion *ex vivo*. **B-C** Representative images of U251-mCherry spheroids stably expressing shControl, shVangl1-1, shVangl1-2, or shVangl1-3 **(B)** or shControl, shFzd7-1, or shFzd7-2 **(C)**, 72 hours after implantation into mouse brain slices. Scale bar=100μm. **D-E** Invaded U251-mCherry spheroids stably expressing shControl, shVangl1-1, shVangl1-2, or shVangl1-3 (*n*=4) were assessed for the relative distance (t-test: *p*=0.0129, *p*=0.0101, and *p*=0.0099; ANOVA: *p*=0.0107, *p*=0.0002, and *p*=0.0007). **(D)**, and the relative number of (t-test: *p*=0.0178, *p*=0.0151, and *p*=0.0165; ANOVA: *p*=0.0039, *p*=0.0099, and *p*=0.0066) **(E)** cells invaded out of the spheroids into the surrounding brain tissue. **F-G** Invaded U251-mCherry spheroids stably expressing shControl, shFzd7-1, or shFzd7-2 were assessed for the relative distance (*n*=3 or 4, t-test: *p*=0.0384, and *p*=0.0335; ANOVA: *p*=0.0861, and *p*=0.0064) **(F)**, and the relative number of (*n*=3 or 4, t-test: *p*=0.0262, and *p*=0.0019; ANOVA: *p*=0.0001, and *p*=0.0004) **(G)** cells invaded out of the spheroids into the surrounding brain tissue. Errors bars depict SEM. Statistical significance was calculated using an unpaired two-tailed t-test with Welch's correction or one-way ANOVA with multiple comparisons.
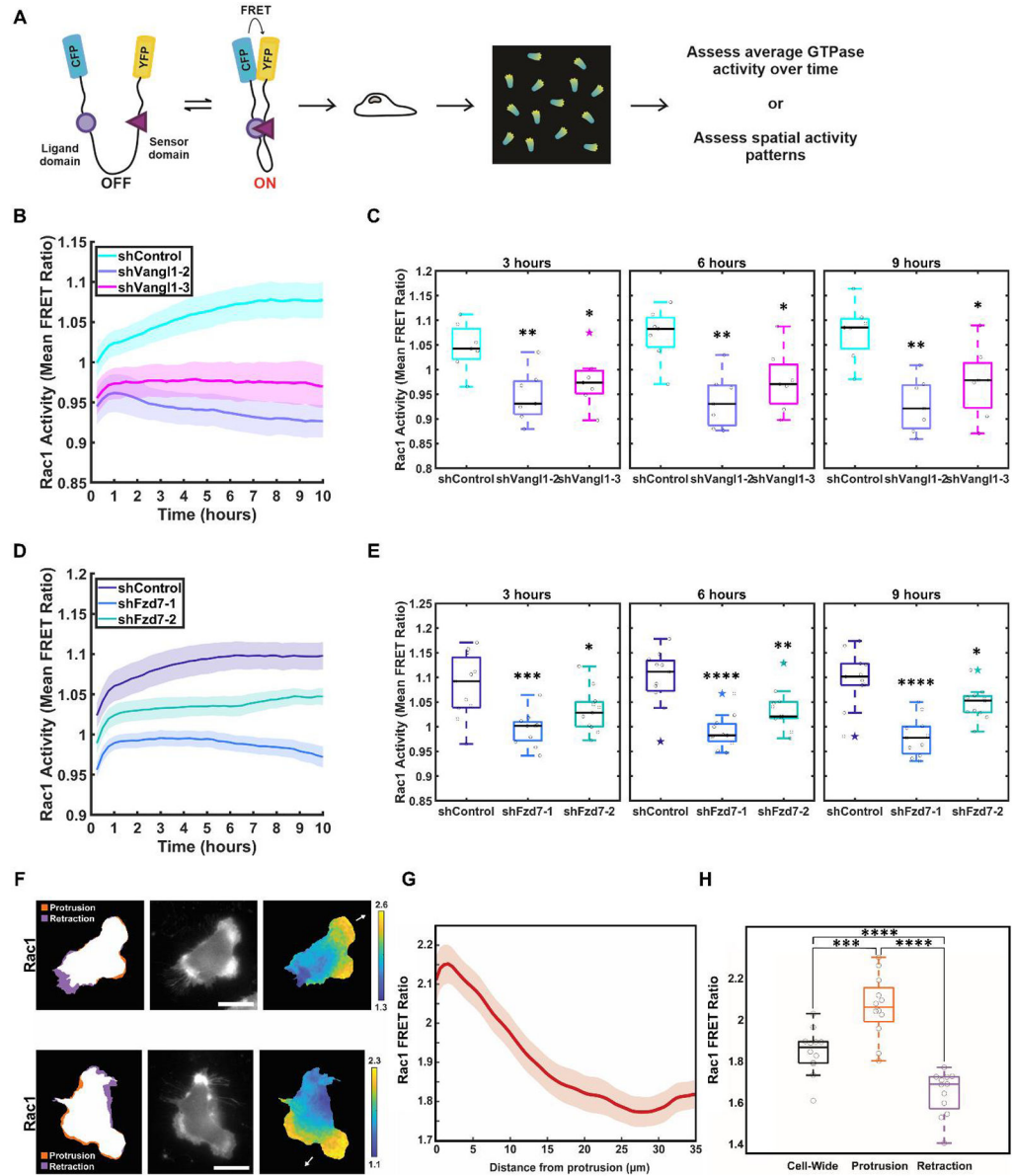
Figure 3. Rac1 activity is localized to the leading edge of migratory GBM cells and is regulated by Vangl1 and Fzd7.

A Schematic representation of the experimental design employed to assess Rac1 and RhoA activity and spatial patterning. **B** Average Rac1 activity in migrating U251 cells stably expressing shControl, shVangl1-2, or shVangl1-3 normalized to 0 hour. Shaded error bars indicate ± sem of *n*=7. **C** Average Rac1 activity of U251 cells stably expressing shControl, shVangl1-2, or shVangl1-3 at 3 hours, 6 hours, and 9 hours of migration (*n*=7) (3 hours: *p*=0.0030, and *p*=0.0284; 6 hours: *p*=0.0060, and *p*=0.0116; 9 hours: *p*=0.0030, and 0.0127). **D** Average Rac1 activity in migrating U251 cells stably expressing shControl, shFzd7-1, or shFzd7-2 normalized to 0 hour. Shaded error bars indicate ± sem of *n*=11. **E** Average Rac1 activity of U251 cells stably expressing shControl, shFzd7-1, or shFzd7-2 at 3 hours, 6 hours, and 9 hours of migration (*n*=11) (3 hours: *p*=0.0008, and *p*=0.0485; 6 hours: *p*=3.286E-05, and *p*=0.0083; 9 hours: *p*=1.225E-05, and 0.0175). **F** Representative high

magnification images of U251 cells stably expressing the Rac1 FRET biosensor depicting active cellular protrusions (orange) and retractions (purple) (left panel), grey scale of fluorescent intensity (middle panel), and spatial activity profiles of Rac1 activity (left panel). Color bars indicate range of Rac1 FRET activity ratios. Scale bar=25μm. **G** Average Rac1 activity in migratory U251 cells as a function of distance from the leading edge of the cell. Shaded error bars indicate ± sem of n=12 cells. **H** Box plots comparing the average Rac1 FRET ratios cell-wide and within protrusions or retractions in migratory U251 cells (cell-wide vs protrusion p=0.002, cell-wide vs retraction p=0.0003, protrusion vs retraction p=0.000037). Statistical significance was calculated using a paired t-test **(B,D)**, or Mann-Whitney **(H)**.
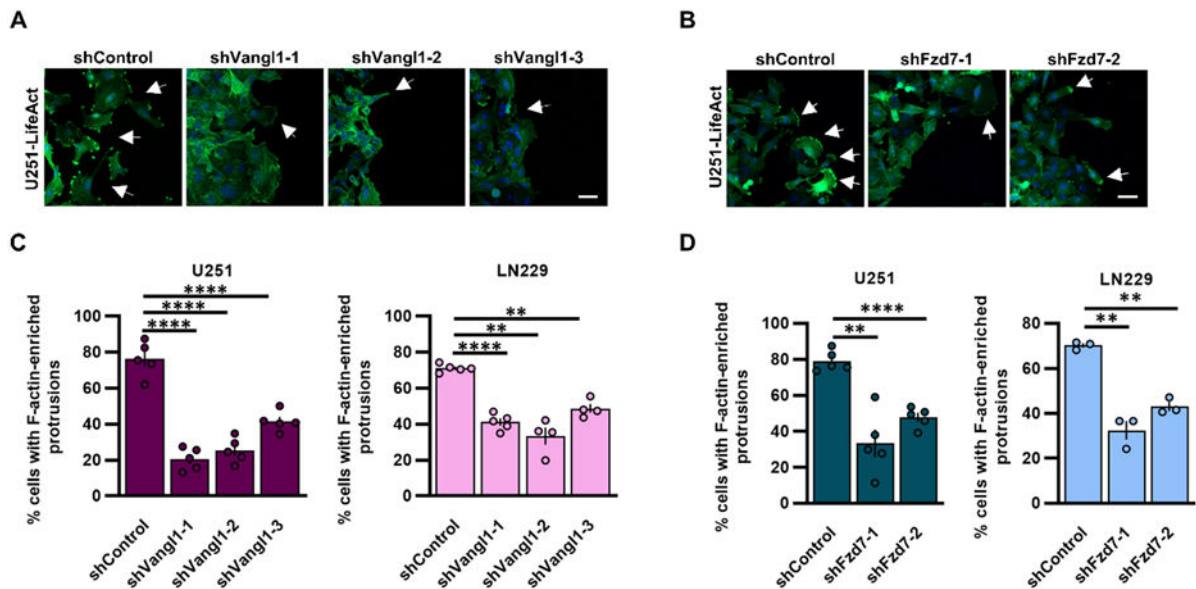
Figure 4. Vangl1 and Fzd7 mediate actin dynamics in migrating GBM cells.
A-B Representative images of migrating U251 cells stably expressing LifeAct-GFP
and shControl, shVangl1-1, shVangl1-2, or shVangl1-3 **(A)** or shControl, shFzd7-1, or
shFzd7-2 **(B)**, LifeAct: green, DAPI: blue. White arrows: cells with F-actin-enriched
migratory protrusions. Scale bar=50μm. **C-D** Quantification of the percentage of F-actin-
enriched protrusions at the leading edge of a scratch in U251- or LN229-LifeAct-GFP
cells stably expressing shControl, shVangl1-1, shVangl1-2, or shVangl1-3 (U251, n=5:
t-test: p=2.054E-07, p=1.366E-06, and p=2.798E-05, ANOVA: p<0.0001, p<0.0001, and
p<0.0001; LN229, n=4 or 5: t-test: p=1.479E-05, p=0.0033, and p=0.0012, ANOVA:
p<0.0001, p<0.0001, and p=0.0001) **(C)** or shControl, shFzd7-1, or shFzd7-2 (U251, n=5:
t-test: p=0.0027, and p=2.310E-05, ANOVA: p<0.0001, and p=0.0014; LN229, n=3: t-test:
p=0.0086, and p=0.0013, ANOVA: p=0.0001, and p=0.0007) **(D)**. Errors bars depict SEM.
Statistical significance was calculated using an unpaired two-tailed t-test with Welch's
correction or ordinary one-way ANOVA with multiple comparisons.
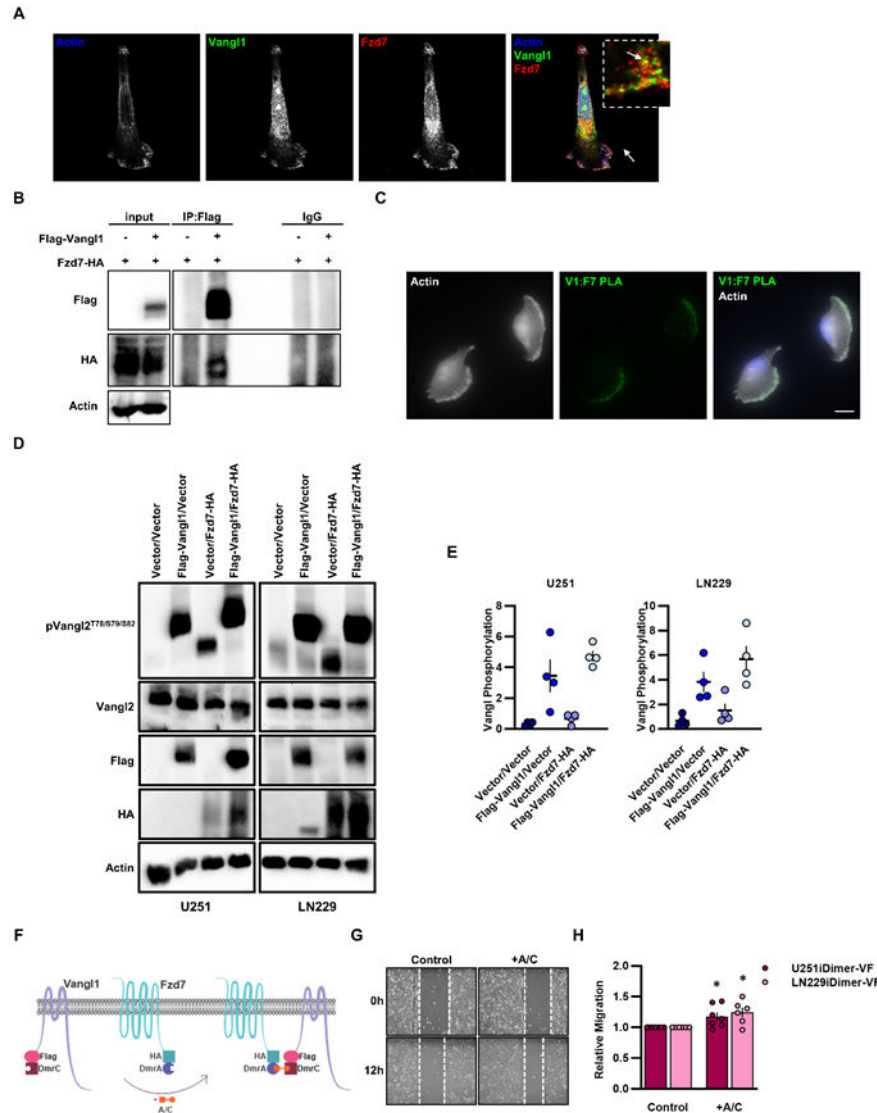
Figure 5. Vangl1 and Fzd7 form a complex at the leading edge of migratory GBM cells to mediate downstream cellular outcomes.

A Representative confocal images of migratory U251 cells stained for Actin: blue, Vangl1: green, Fzd7: Red, and DAPI: blue. White arrows: yellow puncta indicative of overlapping staining of Vangl1 and Fzd7. Scale bar=10μm. **B** HEK293T cells were transfected with Fzd7-HA alone or Flag-Vangl1 and Fzd7-HA, and anti-Flag precipitates were blotted for Flag and HA. **C** Representative images of *in situ* Vangl1:Fzd7 interactions using PLA in migratory U251-LifeAct cells. LifeAct: white, Vangl1:Fzd7 PLA: green, DAPI: blue. Scale bar=20μm. **D-E** U251 and LN229 cells stably overexpressing Vector/Vector, Flag-Vangl1/Vector, Vector/Fzd7-HA, or Flag-Vangl1/Fzd7-HA immunoblotted for phosphorylated Vangl (lower band=endogenous, upper band=ectopic) **(D)** and quantification of Vangl phosphorylation levels (*n*=4) (U251: Vector/Vector vs Flag-Vangl1/Vector *p*=0.0102, Vector/Vector vs Vector/Fzd7-HA *p*=0.9749, Vector/Vector vs Flag-Vangl1/Fzd7-HA *p*=0.0007, Flag-Vangl1/Vector vs Vector/Fzd7-HA *p*=0.0211, Flag-Vangl1/Vector vs Flag-Vangl1/Fzd7-HA *p*=0.4097, and Vector/Fzd7-HA vs Flag-Vangl1/Vector *p*=0.0013; LN229: Vector/

Vector vs Flag-Vangl1/Vector p=0.0500, Vector/Vector vs Vector/Fzd7-HA p=0.8594, Vector/Vector vs Flag-Vangl1/Fzd7-HA p=0.0025, Flag-Vangl1/Vector vs Vector/Fzd7-HA p=0.1830, Flag-Vangl1/Vector vs Flag-Vangl1/Fzd7-HA p=0.3458, and Vector/Fzd7-HA vs Flag-Vangl1/Vector p=0.0094) **(E). F** Schematic representation of the iDimerize inducible heterodimer system used to force a constitutive interaction between Vangl1 and Fzd7. **G** Representative images of migrating LN229iDimer-VF cells treated with Control or A/C at 0 and 12 hours. **H** Quantification of relative migration of U251iDimer-VF and LN229iDimer-VF cells treated with Control or A/C (U251iDimer-VF: n=7, p=0.0387; LN229iDimer-VF: n=6, p=0.0263). Errors bars depict SEM. Statistical significance was calculated using an unpaired two-tailed t-test with Welch's correction or ordinary one-way ANOVA with multiple comparisons. Images and immunoblots are representative from at least 4 independent experiments.
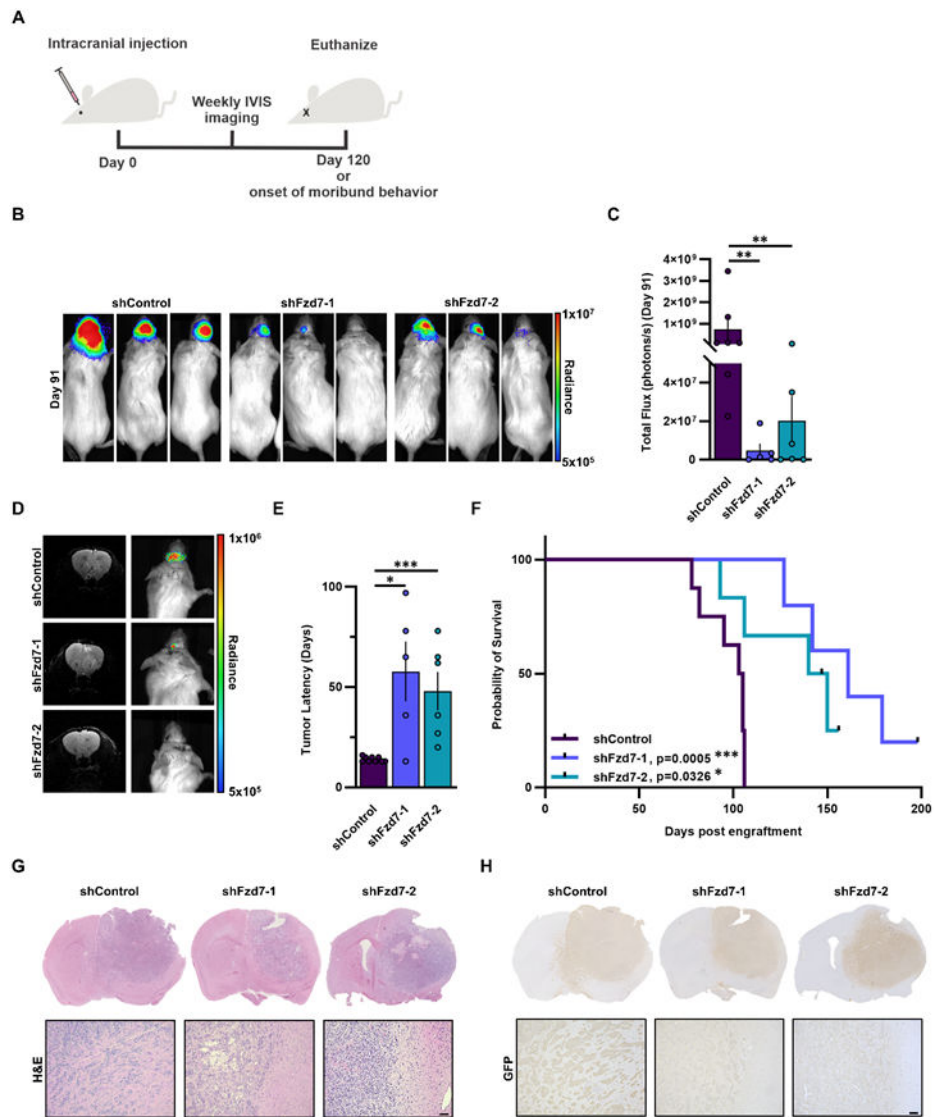
Figure 6. Fzd7 depletion suppresses GBM growth and aggressiveness and extends overall survival *in vivo*.

A Study design depiction of the *in vivo* study employed to assess the role of Fzd7 in mediating GBM progression. **B-F** Representative images and plots depicting tumor growth characteristics of NOD SCID mice bearing intracranial U251-luciferase-GFP tumors stably expressing shControl (*n*=7), shFzd7-1 (*n*=5), or shFzd7-2 (*n*=6). Representative bioluminescence images at 91 days post-engraftment **(B)**, average signal intensity (flux=photons per second) at 91 days post-engraftment (*p*=0.0025 and *p*=0.0082) **(C),** representative images of T2-weighted MRI scans at 60 days post-engraftment, average tumor latency (*p*=0.0170 and *p*=0.0002) **(E)**, and Kaplan-Meier survival curves (*p*=0.0005 and *p*=0.0326) **(F)**. **G-H** Representative images of U251-luciferase-GFP tumors stably expressing shControl, shFzd7-1, or shFzd7-2 stained for hematoxylin and eosin (H&E) **(G)**, and GFP **(H)**. High magnification images depict tumor borders. Scale bar=100μm. Errors bars depict SEM. Statistical significance was determined by Mann-Whitney **(C, E)**, or Log-rank **(F)**.
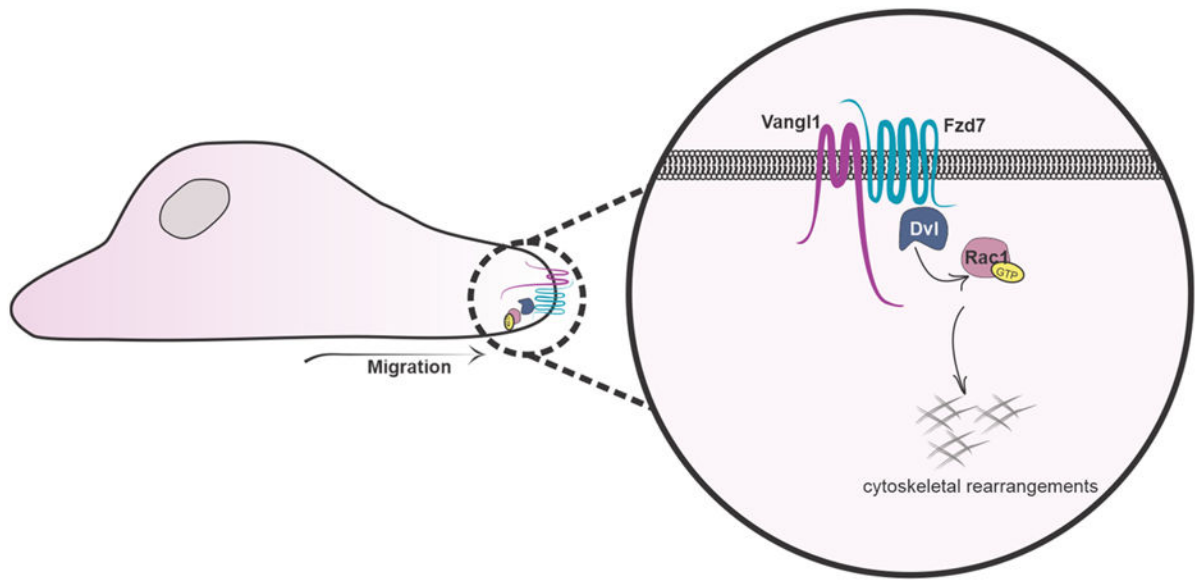
Figure 7. Model of Wnt/PCP components Vangl1 and Fzd7 coordinating downstream signaling and actin cytoskeletal dynamics to drive GBM aggressiveness.
Vangl1 and Fzd7 localize to and interact at the leading edge of migratory GBM cells where they engage and recruit downstream components Dvl2 and Rac1 to drive cytoskeletal rearrangements necessary for successful cellular proliferation, migration, and invasion.